An explicit estimate of the atmospheric nutrient impact on global oceanic productivity

Stelios Myriokefalitakis[1], Matthias Gröger[2], Jenny Hieronymus[3] and Ralf Döscher[3]

[1] Institute for Environmental Research and Sustainable Development (IERSD), National Observatory of Athens, Penteli,
Greece
[2] Leibniz Institute for Baltic Sea Research Warnemünde (IOW), Rostock, Germany
[3] Swedish Meteorological and Hydrological Institute (SMHI), Norrköping, Sweden

Correspondence to: Stelios Myriokefalitakis (steliosm@noa.gr) and Matthias Gröger (matthias.groeger@io-warnemuende.de)

Abstract. State-of-the-art global nutrient deposition fields are here coupled to the biogeochemistry model PISCES to investigate the effect on ocean biogeochemistry in the context of atmospheric forcings for preindustrial, present, and future periods. Present-day atmospheric deposition fluxes of inorganic N, Fe, and P over the global ocean are accounted equal to ~40 Tg-N yr^{-1}, ~0.28 Tg-Fe yr^{-1} and ~0.10 Tg-P yr^{-1}. The resulting globally integrated primary production of roughly 47 Pg-C yr^{-1} is well within the range of satellite-based estimates and other modeling predictions. Preindustrial atmospheric nutrient deposition fluxes are lower compared to present-day (~51%, ~36%, and ~40% for N, Fe, and P, respectively), resulting here in a lower marine primary production by ~3% globally. Future changes in air pollutants under the RCP8.5 scenario result in a modest decrease of the bioaccessible nutrients input into the global ocean compared to present-day (~13%, ~14% and ~20% for N, Fe and P, respectively), without significantly affecting the projected primary production in the model. The global mean nitrogen-fixation rates changed only marginally from preindustrial to future conditions (111±0.6 Tg-N yr^{-1}). With regard to the atmospheric inputs to the ocean, sensitivity model simulations indicate that the contribution of nutrients' organic fraction results in an increase in primary production by about 2.4%. This estimate is almost equal to the effect of emissions and atmospheric processing on the oceanic biogeochemistry since preindustrial times in the model, when only the inorganic fraction of the nutrients is considered. Although the impact of the atmospheric organic nutrients may imply a relatively weak response of marine productivity on a global scale, stronger regional effects up to ~20% are calculated in the oligotrophic subtropical gyres. Overall, this work provides a first explicit assessment of the contribution of the organic forms of atmospheric nutrients, highlighting the importance of their representation in biogeochemistry models and thus the oceanic productivity estimates.

1 Introduction

Marine primary production is a critical component of the global carbon cycle and important for sustaining the habitability on Earth, but vulnerable to environmental changes (e.g., Steinacher et al., 2010). For example, an estimated decline of subarctic productivity has been reported to accompany the warming of the last 150 years (Osman et al., 2019). Global warming induced

5   by greenhouse gas emissions has increased ocean stratification, reducing the supply of nutrients from subsurface waters and inhibiting the growth of phytoplankton in the surface ocean (Behrenfeld et al., 2006), highlighting thus the role of nutrient supply by atmospheric deposition to the ocean. Several studies have documented the importance of primary production on the surface ocean CO_2 concentrations (e.g., Falkowski et al., 2000; Gruber, 2004; Gruber et al., 2009; Le Quéré et al., 2013; Smith, 2019) via carbon uptake and sinking of the particulate organic matter to the deeper ocean. However, significant uncertainties

10   remain in the projected export production among state-of-the-art model simulations which can range between 2 and 20% for CMIP3 and CMIP5 models (Fu et al., 2016; Steinacher et al., 2010), mainly due to the different responses of phytoplankton production to changes in water temperature and stratification (e.g., Gröger et al., 2013; Laufkötter et al., 2016).

During primary production, the growth of the phytoplankton functional types (e.g., diatoms and nano-phytoplankton) results in a newly formed particulate organic matter within the euphotic zone. These processes are limited however by light,

15   temperature, and nutrients' availability. Human activities have heavily perturbed the atmospheric chemical composition (e.g., Mahowald et al., 2017), but the impact of atmospheric composition on marine biogeochemistry and consequently on the oceanic carbon- and nutrient-cycles is rather complex and still not fully understood. Among other species deposited into the open ocean, nitrogen (N), iron (Fe), and phosphorus (P) are the nutrients that significantly limit the marine phytoplankton growth rates and thus directly impact on ocean-atmosphere carbon fluxes, in particular where the nutrients are the growth-

20   limiting factor for phytoplankton.

Atmospheric nitrogen inputs to the global ocean are mainly derived from anthropogenic combustion and agricultural sources over densely populated regions (Duce et al., 2008). So far, it is widely accepted that the marine biota primarily utilizes the inorganic nitrogen in its oxidized form (i.e., nitrogen oxides (NOx), nitric acid (HNO_3) and particulate nitrate (NO_3^-)), as well as in its reduced form (i.e., ammonia (NH_3) and particulate ammonium (NH_4^+)) (e.g., Duce et al., 1991). However, there is

25   evidence that the dissolved organic nitrogen (DON) inputs (e.g., from rivers along the coasts) can likewise be also efficiently utilized (e.g., Aumont et al., 2015). In the atmosphere, the global organic nitrogen (ON) cycle has a strong (~45%) anthropogenic component (Kanakidou et al., 2012). Kanakidou et al. (2016) calculated that 20%–25% of the nitrogen deposition is in the form of ON, overall with DON deposition to be about 25% of the total dissolved nitrogen deposition to the global ocean.

30   Present-day atmospheric nitrogen input to the oceans is estimated to be roughly 39-68 Tg-N yr^{-1} (e.g., Duce et al., 2008; Kanakidou et al., 2016; Krishnamurthy et al., 2007; Wang et al., 2019), with the global oxidized and reduced nitrogen flux having increased from the preindustrial values of ~13 Tg-N yr^{-1} to about 40 Tg-N yr^{-1} in modern times (Kanakidou et al., 2016). Moreover, the aforementioned authors suggested that nearly half of nitrogen emissions are processed into aerosols in

the atmosphere, with the nitrogen-containing aerosols having increased by approximately 2.5 times since preindustrial times; overall, corresponding to a ~2 times increase of atmospheric soluble N deposition in the ocean due to human activities alone. Atmospheric nitrogen deposition may also significantly impact on the surface water inorganic N/P ratios and thus further influence global nitrogen fixation rates (Moore and Doney, 2007), i.e., the reduction of gaseous N_2 to ammonium as catalyzed

5   by nitrogenase. Krishnamurthy et al. (2007) also demonstrated that compared to preindustrial conditions, present-day inorganic nitrogen inputs to the oceans from anthropogenic sources could so far be partially compensated by the decreased nitrogen fixation, resulting thus in a modest effect on primary production.

The most important atmospheric source for marine nutrients (such as Fe, P, and Si) in the open ocean is the mineral dust deposition. Dust aerosols are usually subject to intensive atmospheric processing during their long-range transport over remote

10 oceanic regions. Changes in the properties of mineral aerosols during atmospheric transport involve chemical interactions with air masses (i.e., aerosol aging) that lead to different coatings of dust particles by sulfate (SO_4^{2-}), NH_4^+, NO_3^-, and organics (e.g., oxalic acid). In particular, pollutants increase the atmospheric acidity via the formation of strong acids, such as the sulfuric (H_2SO_4) and nitric (HNO_3) acids, that coat deliquesced minerals and eventually transform part of their contained insoluble forms (e.g., hematite, apatite) into soluble forms (e.g., Fe(II), Fe(III), PO_4^{-3}) during atmospheric processing (e.g., Nenes et al.,

15 2011; Shi et al., 2011). This process is further enhanced in the presence of organics such as the oxalic acid, that converts part of the insoluble Fe-containing minerals to soluble organic Fe-complexes, under favored atmospheric conditions (e.g., Paris et al., 2011; Paris and Desboeufs, 2013). However, according to future emission scenarios (van Vuuren et al., 2011), the sources of the main acidic atmospheric species such as the nitrogen oxides (NOx) and sulfur (SOx) are expected to decrease by 34–59% and 75–88%, respectively, from 2010 to 2100, but ammonia (NH_3) will increase by 3–55%. This heterogeneity in the

20 projection of acidic and alkaline emissions is expected to no-linearly perturb the atmospheric aerosol acidity (Weber et al., 2016), making overall the atmosphere-ocean interactions even more complex.

Both iron and phosphorus are utilized by marine phytoplankton mainly in their dissolved forms, although the actual bioavailability may substantially differ from the soluble forms of the deposited nutrients into the ocean (Meskhidze et al., 2019). For example, Rubin et al. (2011) showed that in the tropical and subtropical Atlantic Ocean, some marine organisms

25 (e.g., the *Trichodesmium*) can access directly the mineral (insoluble) particulate iron. In addition, emissions of dissolved Fe (DFe) and dissolved P (DP) from anthropogenic combustion and biomass burning processes can contribute significantly to the atmospheric inputs into the ocean (e.g., Barkley et al., 2019; Matsui et al., 2018). However, the aerosols from natural and combustion sources tend to be deposited in different regions of the oceans; for example, the subtropical North Atlantic Ocean and the Arabian Sea receive the majority of Fe originated from dust aerosols, in contrast to the Pacific and Southern oceans

30 where the Fe-containing combustion aerosols are mainly deposited (Ito et al., 2019b).

Present-day global atmospheric DFe and DP deposition fluxes into the ocean are calculated in the range 0.2–0.4 Tg-Fe yr^{-1} (Ito et al., 2019a; Myriokefalitakis et al., 2018) and 0.10-0.17 Tg-P yr^{-1} (Mahowald et al., 2008; Myriokefalitakis et al., 2016), respectively. Myriokefalitakis et al. (2016) presented a comprehensive description of the organic forms of P (i.e., soil's organic matter, OP associated with anthropogenic combustion and biomass burning emissions, as well as from primary biological

aerosol particles). They also demonstrated that DOP can contribute to DP more than 50% over the equatorial oceanic regions. Compared to present day, DP and DFe emissions may have increased by roughly 3 and 6 times respectively, since 1850 (Myriokefalitakis et al., 2015, 2016). Wang et al. (2014) further showed that DP emissions increased due to the extended use of biofuels in the energy production sector in developing countries as well as emissions due to extensive deforestation in South

5   America and Southeast Asia. By contrast, a significant increase for DFe emissions before the 1990s due to coal combustion is calculated, followed-up by a decline due to the implementation of air-pollution abatements (Wang et al., 2015b).

Primary production is currently estimated in the order of 44 - 67 Pg-C yr^{-1}, based on biogeochemistry calculations and satellite-based estimates (e.g., Aumont et al., 2015; Behrenfeld et al., 2005; Gröger et al., 2013; Krishnamurthy et al., 2007, 2009, 2010; Steinacher et al., 2010). The primary production is, however, strongly linked to nitrogen and iron acquisitions by marine biota,

10   with modelling estimates to indicate an increase for present-day values since preindustrial times (Krishnamurthy et al., 2009). The surface oceanic nutrient concentrations, however, are strongly impacted by the atmospheric deposition on a regional scale. Nitrogen atmospheric inputs were shown to have a significant effect on marine productivity, export production, and carbon uptake in Low-Nutrient-Low-Chlorophyll (LNLC) regions. It has been also suggested that the simultaneous anthropogenic N and Fe deposition can increase oceanic productivity by 1.5 Pg-C yr^{-1}, corresponding overall to a reduction of atmospheric

15   pCO$_2$ level by ~2.2 ppm by the year 2100 (Krishnamurthy et al., 2010). Assuming, however, complete assimilation of anthropogenic nitrogen by carbon fixation, a new marine biological production up to 0.3 Pg-C yr^{-1} can be also supported (Duce et al., 2008). Although P deposition may account for only a small fraction of export production (Krishnamurthy et al., 2010), an increase in Fe and P deposition can further enhance the N$_2$-fixation in LNLC oceans (Mahowald, 2011; Moore et al., 2013b). A large portion of the global ocean, especially the subtropical gyres, is depleted in nitrate and phosphate, and consequently,

20   sustain a low growth of phytoplankton and other marine organisms (e.g., Moore et al., 2013a). About 40% of the global ocean is estimated to be N-limited (Krishnamurthy et al., 2009; Wang et al., 2015a), with most of the remaining to be Fe-limited. The relative larger increases in N than P deposition fluxes in many regions of the globe cause shifts from N to P limitation (Krishnamurthy et al., 2009; Moore et al., 2013a). Many studies suggest that anthropogenic Fe deposition is the most important factor for carbon uptake (Krishnamurthy et al., 2010; Okin et al., 2011), mainly due to the potential to increase productivity in

25   High-Nutrient-Low-Chlorophyll (HNLC) regions. On the other hand, a number of studies argue that anthropogenic N deposition is equally important for ocean biogeochemistry (Duce et al., 2008; Wang et al., 2015a). The essential role of iron in oceanic productivity is, however, well established (Tagliabue et al., 2017) and currently routinely included in biogeochemistry modelling studies (e.g., Aumont and Bopp, 2006; Hajima et al., 2019; Ito et al., 2019b; Moore et al., 2001; Tagliabue et al., 2014, 2016). Nitrogen fixation rates are also sensitive to atmospheric Fe inputs (Camarero and Catalan, 2012;

30   Schulz et al., 2012) since N$_2$-fixing species (diazotrophs) have elevated Fe requirements. For example, the N$_2$-fixation is suppressed due to iron-limitations in the eastern tropical Pacific (Wang et al., 2019). Present-day global nitrogen fixation is currently estimated in the range of ~111-163 Tg-N yr^{-1} (e.g., Aumont et al., 2015; Krishnamurthy et al., 2009; Wang et al., 2019). Wang et al. (2019) suggested that roughly half of the export production in the subtropical gyres is due to the nitrogen from microbial fixation and external inputs, such as rivers and atmospheric deposition. With regard to the atmospheric inputs,

the aforementioned study also demonstrated by inversion calculations a potential decrease (~10%) of N_2-fixation, as a response to the elevated present-day nitrogen emissions.

The aim of the present study is to analyze the impact of a detailed representation of atmospheric inputs to the oceanic productivity. For this, a state-of-the-art biogeochemical model is used to integrate the recent knowledge of the atmospheric nutrient deposition fluxes into the ocean, driven by natural and combustion emissions, along with the contribution of the atmospheric processing. The outlined variable composition and varying sources of the deposited nutrients (i.e., N, Fe, and P) used in this work, have been recently modeled with a state-of-the-art atmospheric chemistry and transport model based on preindustrial, present, and future emissions. The description of the biogeochemical model and the parameterizations used in the atmospheric chemistry transport model, related to the calculations of the atmospheric deposition fields of this work, are presented in Sect. 2. A comprehensive description of the regional changes in deposition fluxes and the linked atmospheric processes controlling them is also provided. In Sect. 3, the calculated nutrient oceanic concentrations and the relevant biogeochemical processes, such as the nitrogen fixation and the primary production, are presented and compared to estimates from observations and other modelling studies. The role of present-day air pollutants on nutrients' atmospheric deposition is here discussed via the comparison of experiments that are forced from atmospheric inputs of preindustrial and projected anthropogenic and biomass burning emission scenarios. In particular, the impact of the organic fraction of the deposited nutrients in the global oceanic productivity is also assessed. Finally, the implications of our findings concerning the above biogeochemistry parameters are summarized in Sect. 4.

2 Model description

The state-of-the-art biogeochemistry model PISCES (Aumont et al., 2015), enabled here within the European Earth System Model (ESM) EC-Earth (http://www.ec-earth.org/), is used to investigate the impact of atmospheric deposition fluxes of N, Fe and P on the marine productivity. EC-Earth is a global ESM, with the ECMWF Integrated Forecast System (IFS) and the Nucleus for European Modelling of the Ocean (NEMO) as core components, with PISCES (as part of NEMO) to include a detailed representation of the lower trophic levels of marine ecosystems. PISCES (Pelagic Interactions Scheme for Carbon and Ecosystem Studies volume 2) simulates the biogeochemical cycles of carbon and the main nutrients (N, P, Fe, and Si) and includes external nutrient sources from atmospheric deposition, rivers, sea ice, sediment dissolution, and hydrothermal vents. PISCES includes two types of phytoplankton, namely nanophytoplankton and diatoms, and it simulates the chlorophyll concentrations and the growth of phytoplankton based on nutrients' availability (i.e., DP, DN, and DFe for nanophytoplankton and DP, DN, DFe, and DSi for diatoms), temperature and light. Phytoplankton can be grazed by zooplankton or to enter directly into the detritus pool. All particulate organic matter sinking to the bottom undergoes remineralization in the deeper ocean and the nutrient formerly incorporated during photosynthesis is released again. PISCES simulates the full inorganic carbon cycle including the biological and the carbonate counter pump. At the ocean surface, air-sea gas exchanges for carbon dioxide,

oxygen, and nitrogen are parameterized following Wanninkhof (1992). The model has been successfully tested against the response of oceanic productivity to dust (Guieu et al., 2014) and climatic variability (Schneider et al., 2008).

2.1 Biogeochemistry model set-up

For this study, PISCES uses a ~1° horizontal resolution with a latitudinal grid refinement in the tropics and 75 layers for the

5 ocean (i.e., ORCA R1) and a global timestep of 2700 sec. The model is here forced by dynamical physical outputs from an OMIP simulation (Ocean Modelling Intercomparison Project; Orr et al., 2017), with a repeated interannual (1948-2009) forcing. For the spin up, five iterations were carried out to ensure that the upper ocean biogeochemistry is drift free (Skyllas et al., 2019). For the initialization of the ocean biogeochemical fields, the climatological fields of oxygen, nitrate, silicate, and phosphate from the World Ocean Atlas (WOA; Garcia et al., 2010a, 2010b) and alkalinity from the Global Ocean Data

10 Analysis Project (Key et al., 2004) were adopted.

The default N, Fe and P atmospheric inputs of PISCES in the EC-Earth configuration have been replaced for the present study by state-of-the-art monthly mean atmospheric deposition fields, recently published in the literature. Note that the default PISCES configuration (Aumont et al., 2015) uses yearly resolution N deposition fluxes of ~67 Tg-N yr^{-1} into the global ocean (Duce et al., 2008) assuming that all deposited N into the ocean is dissolved. Respectively, the Fe, P (and Si) atmospheric

15 inputs were calculated from the same (monthly resolution) dust deposition field. Specifically, for the Fe atmospheric input, the Fe content in dust was set to 3.5% and its soluble fraction was derived based on the simulated monthly resolved Fe solubility fields (Luo et al., 2008; Mahowald et al., 2009) overall, resulting in a soluble Fe input to the ocean of ~0.15 Tg-Fe yr^{-1}. For the P atmospheric input, the P content in dust was set globally to 750 ppm and with a constant solubility of 10% (Mahowald et al., 2008), resulting in a DP deposition flux of ~0.02 Tg-P yr^{-1} in the global ocean. In contrast to previous studies (e.g.,

20 Aumont et al., 2015), the new atmospheric deposition fields considered here are all calculated based on:

1) emissions of natural and combustion nutrient containing aerosols,
2) detailed atmospheric gas- and aqueous-phase chemical schemes, and
3) mineral dissolution processes due to atmospheric acidity and organic ligand (oxalic acid) in aerosol water and cloud droplets.

25 Note that no extra optimizations for the iron scavenging parameters have been applied for this work, since the default model set-up already considers a variable iron solubility on the dust deposition inputs (see Aumont et al., 2015 and ref. therein).

Two simulations from 1851 to 2100 were performed to study the impact of nutrients (N, P, and Fe) atmospheric input on global marine productivity:

1) a control simulation (CTRL) accounting for the inorganic fractions of the deposited atmospheric nutrients (N, P, and

30 Fe) into the global ocean, and
2) a sensitivity simulation (ORGF), as for CTRL but also accounting for the organic fractions of the deposited atmospheric nutrients (N, P, and Fe).

We here analyze results for the preindustrial (PAST: 1851–1870 average), present-day (PRESENT: 2001–2020 average), and future projected (FUTURE: 2081–2100 average) periods. Note also that the ocean and biogeochemistry modules used here may slightly differ from the version recently used in EC-Earth CMIP6 simulations since at the time the simulations were carried out the final version of EC-Earth was still not released.

5   For the revised atmospheric deposition rates, a spin-up period of 200 yrs. (i.e., 1651-1850) is here considered for each simulation, to reach a quasi-equilibrium state in the model with a well-ventilated upper ocean and a minimal model drift (i.e., <0.01% difference in the vertically integrated primary production). The monthly atmospheric inputs of nutrients were prescribed to the model, with the deposition fluxes for the spin-up fixed at the levels calculated with the anthropogenic and biomass burning emissions of the year 1850. After the spin-up period, the deposition data were employed as external forcings,

10   linearly interpolated from preindustrial (i.e., the year 1851) up to present-day conditions (i.e., the year 2010) to smoothly capture the transition from preindustrial to the modern conditions as in Krishnamurthy et al. (2009). Respectively, the deposition data from the present day were also linearly interpolated to the projected estimates (i.e., the year 2100). Note that for all temporal and spatial interpolations of this work, the Climate Data Operators (CDO v.1.9.8) software as provided by the Max Planck Institute for Meteorology is used (https://code.mpimet.mpg.de/projects/cdo/embedded/cdo.pdf; last access

15   29/02/2020). For all simulations, the atmospheric CO_2 mixing ratio is set to the pre-industrial value of 284.7 ppm, to effectively isolate the impact of atmospheric deposition on the marine biogeochemistry parameters.

2.2 Atmospheric parameterizations

For this work, all atmospheric nutrient inputs are derived from the global atmospheric Chemistry-Transport Model (CTM) TM4-ECPL. The CTM is driven by the ECMWF (European Centre for Medium – Range Weather Forecasts) Interim re–

20   analysis project (ERA Interim) meteorology (Dee et al., 2011) and uses a horizontal resolution of 3º in longitude by 2º in latitude, with 34 hybrid layers up to 0.1 hPa. The CTM simulates the gas-phase chemistry along with the major non-methane volatile organic compounds, as well as all major aerosol components, such as dust, sea-salt, organic aerosols (OA), black carbon (BC), SO_4^{2-}, NH_4^+, and NO_3^-. The thermodynamic equilibrium model ISORROPIA II (Fountoukis and Nenes, 2007) is used to estimate the water content and the acidity of hygroscopic aerosols, accounting also for the impact of crustal materials

25   (i.e., Ca^{2+}, Mg^{2+}, K^+, Na^+, Cl^-) from mineral dust and sea-salt (Myriokefalitakis et al., 2015). The in-cloud acidity is mainly controlled by strong acids, i.e., sulphuric acid H_2SO_4/SO_4^{2-}, methanesulphonic acid (MSA/MS$^-$), and HNO_3/NO_3^-, and bases (NH_3/NH_4^+), accounting also for the dissociation of hydrated CO_2, sulphur dioxide (SO_2), and oxalic acid (Myriokefalitakis et al. 2011). The CTM further considers the multiphase chemistry secondary aerosol production in cloud droplets and aerosol water (Myriokefalitakis et al., 2011), as well as the secondary organic aerosol (SOA) formation via gas-to-particle partition

30   over land and oceanic regions (e.g., Myriokefalitakis et al., 2010). For the present study, the anthropogenic (including ships and aircraft emissions) and biomass burning emissions from the historical Atmospheric Chemistry and Climate Model Intercomparison Project (ACCMIP) database (Lamarque et al., 2013) are used in the CTM, and the Representative Concentration Pathways 8.5 (RCP8.5) scenario (van Vuuren et al., 2011) is also used for the future conditions. Note that we

use here the latest updates of nutrient atmospheric deposition fields as recently presented in Kanakidou et al. (2020), which are all based on an on-line dust emission scheme (Tegen et al., 2002). As a result, the global dust source for all simulations is here equal to ~1287 Tg yr^{-1} for the year 2010, well comparable to a multimodel estimate of ~1257 Tg yr^{-1} as reported by Huneeus et al. (2011). However, some small differences on the total amount of deposited nutrients over the ocean are expected

5   compared to previously published results (e.g., Kanakidou et al., 2016; Myriokefalitakis et al., 2015, 2016), due to the various updates of the code, the different year of simulation, or even the different definitions of the oceanic regions due to the applied horizontal analysis in PISCES (i.e., ORCA R1).

2.2.1 Nitrogen

For the calculation of the atmospheric nitrogen cycle, the CTM uses primary emissions of NOx, NH$_3$, marine amines, and
10   emissions of particulate organic nitrogen (ON) from natural and anthropogenic sources (Kanakidou et al., 2012, 2016, 2018). The particulate ON is linked to the OA tracers using varying N:C molar ratios (Kanakidou et al., 2012), as well as to the SOA formation under high NOx-to-VOC conditions (Myriokefalitakis et al., 2010; Tsigaridis et al., 2006). Amines of marine origin in the gas phase are also considered to form amine salts (Myriokefalitakis et al., 2010). A more detailed description of the N-cycle parameterization in the CTM can be found in Kanakidou et al. (2016, 2018).

15   Figure 1 presents the annual mean spatial distribution of dissolved nitrogen deposition as considered in PISCES for the CTRL simulation. The present-day DIN deposition fluxes into the global ocean are estimated to be ~40 Tg-N yr^{-1} (Table 1). DIN deposition (oxidized and reduced inorganic nitrogen) shows the highest fluxes downwind industrial areas of the Northern Hemisphere and the tropical biomass burning regions due to the enhanced NOx emissions, as well as downwind Europe, China, and Indonesia reflecting the high strength of NH$_3$ emissions in these regions. DIN deposition exceeds $1 \cdot 10^{-3}$ kg-N m^{-2} yr^{-1}
20   downwind the eastern United States, Europe, India, China, and Indonesia (Fig. 1b). Some low DIN deposition fluxes over the remote ocean are related to the recycling of the marine NH$_3$ sources. Moreover, when the ON is accounted for the dissolved nitrogen deposition as considered in the ORGF simulation (Fig. S1a), much higher nitrogen deposition fluxes are calculated in the tropics mainly due to the large contribution by primary biogenic particles, the biomass burning emissions, along with the ON production during SOA formation (Fig. S1b). For clarity, we note that for the ORGF simulation, the total ON is
25   assumed as readily bioaccessible in the PISCES, following the previous assumptions for the atmospheric nitrogen inputs to the ocean (Aumont et al., 2015). Note, however, that the total present-day dissolved nitrogen deposition estimate (~58 Tg-N yr^{-1}; Table 1) for the ORGF simulation is lower compared to the N deposition fluxes account for ~67 Tg-N yr^{-1} as taken from Duce et al. (2008) and used in previous PISCES configurations (Aumont et al., 2015).

Compared to the present day, almost all ocean basins (except some parts of the South Indian and the South Pacific Ocean)
30   display a substantially lower (>50%) nitrogen deposition flux during the preindustrial era (Fig. 1a). Inorganic nitrogen inputs to the ocean have significantly increased for present-day along the coasts of the African, Australian, and the South American continents, downwind densely populated areas in the northern hemisphere, such as the east coast of North America and Europe, as well as regions with intensive agriculture downwind the coast of East and South Asia (Kanakidou et al., 2016). Globally,

present-day atmospheric inorganic nitrogen inputs to the ocean have increased by a factor of ~2 since 1850 (Table 1) due to the respective increase of NH_3 and NO_x emissions. The projected atmospheric DIN inputs to the ocean indicate also a decrease (~15%), although much less significant compared to preindustrial times (Table 1) since the reduction in NOx emissions is projected to be compensated by the continuing increase in NH_3 emissions. Note that although the preindustrial ON deposition

5   fluxes into the ocean are estimated to be roughly of the same magnitude as the inorganic nitrogen oceanic input (i.e., ~15 vs. ~20 Tg-N yr^{-1}; Table 1), projections under the RCP8.5 scenario indicate that NHx emissions will gain in importance, resulting overall in a weaker contribution of the oxygenated inorganic nitrogen to the atmospheric deposition into the ocean for future conditions.

2.2.2 Iron

10   The global atmospheric Fe cycle is parameterized in the CTM considering primary Fe emissions associated with minerals in dust and combustion processes. The Fe content of dust minerals is based on detailed mineralogy maps (Nickovic et al., 2012), accounting also for an initial soluble Fe content in the mineral emissions (Ito and Xu, 2014), overall resulting in a mean Fe content in dust emissions of about 3.2%. For the Fe-containing combustion aerosols, the CTM accounts for emissions from biomass burning, coal, and oil combustion (Ito, 2013; Luo et al., 2008) with dissolved Fe contents of 12% for biomass-burning,

15   8% for coal combustion and 81% for oil combustion from shipping Fe emissions. The CTM further accounts for acid- and organic ligand-solubilizations of dust aerosols, in both aerosol and cloud water, as well as for the ageing (i.e., the conversion of insoluble to soluble) of the Fe-containing combustion aerosols via atmospheric processing. More details on the atmospheric Fe-cycle set-up can be found in (Myriokefalitakis et al., 2015, 2018) along with updates from Kanakidou et al. (2020). Figure 1e presents the annual mean spatial distribution of dissolved iron deposition fluxes, as considered from PISCES for the

20   CTRL simulation. DFe deposition fluxes into the ocean present strong spatial variability (Fig. 1e) with an annual flux of ~0.28 Tg-Fe yr^{-1} for the CTRL and ~0.35 Tg-Fe yr^{-1} for the ORGF simulation (Table 1), both estimates are well in range of the mean DFe deposition flux into the ocean (0.2-0.4 Tg-Fe yr^{-1}) as derived from the GESAMP model intercomparison study (Myriokefalitakis et al., 2018). The highest annual mean DFe deposition fluxes into the ocean (Fig. 3c) occur downwind dust source regions with high deposition rates also in the outflow of tropical biomass burning regions (i.e., Central Africa and

25   Indonesia), reflecting the importance of combustion processes. Annual mean DFe deposition rates of ~10^{-5} kg-Fe m^{-2} yr^{-1} are considered for the tropical Atlantic Ocean, as well as, for the Indian Ocean under the influence of the Arabian and Indian peninsulas. For the Southern Ocean, the DFe atmospheric inputs (up to 10^{-6} kg-Fe m^{-2} yr^{-1}) are mainly associated with the Patagonian, the Southern African, and Australian deserts. Figure S1c further presents the annual mean DFe deposition fluxes into the ocean when the organic fraction is considered. The organic bound Fe is produced in the model during the organic-

30   ligand dust dissolution processes, and also accounted for the combustion emissions by considering here a fixed 0.01% fraction (Kanakidou et al., 2018; Myriokefalitakis et al., 2018). Note that although this estimate is highly uncertain due to the lack of observational data and it overall appears to contribute modestly to the global DFe atmospheric input to the ocean (~0.07 Tg-Fe yr^{-1}), it can be potentially important (~up to 40%) in the remote tropical Pacific and the Southern Ocean (Fig. S1d), where

the atmospheric Fe concentrations are extremely low, mainly occurring due to biomass burning and anthropogenic (i.e., ship) combustion emissions (Ito et al., 2019a).

The CTM accounts for increases in DFe deposition rates since preindustrial times, as stronger Fe combustion emissions and a more efficient dust dissolution rate due to the more acidic modern environment occur in the modern era; overall, accounting

5   for about 1.5 times higher DFe atmospheric input to the global ocean for present-day (Table 1). On the other hand, changes in anthropogenic emissions and air-quality are projected to weaken, with the derived DFe in the ocean for the future atmosphere to be ~14% lower than the present-day conditions (Table 1). For the preindustrial era, the largest differences in atmospheric DFe deposition fluxes compared to present-day are considered in the Northern Indian, the North Pacific, and the tropical North Atlantic Oceans (Fig. 1d). Lower atmospheric DFe deposition compared to present-day is also simulated in remote oceanic

10   regions away from dust plumes, in the tropical and subtropical Pacific Ocean, due to the increased present-day atmospheric processing. The combustion source of DFe turns out to be rather important near industrial and biomass burning sources, such as downwind the South and East Asia, where dust emissions are lower. For the future emissions, smaller changes are calculated with a general decrease of the atmospheric DFe input in most parts of the global ocean (Fig. 1f), except for some increases in the Eastern North Pacific Ocean and over the very low atmospheric Fe concentrations regions in the remote Southern Ocean.

15   Note, however, that the calculated increases in the past (and future) deposition fluxes over remote oceanic regions with low atmospheric Fe concentrations, such as the Southern Ocean or downwind strong biomass burning and anthropogenic coal combustion regions, are due to both the relative changes in emission strengths and the impact of atmospheric processing on the dissolved Fe lifetime (Myriokefalitakis et al., 2018).

2.2.3 Phosphorus

20   The atmospheric P-cycle is calculated based on emissions of insoluble mineral P, phosphate, and insoluble and soluble organic P (OP), with the resulted DP deposition fluxes in the CTM being driven by natural (i.e., dust, bioaerosols, sea spray and, volcanic aerosols) and combustion P-containing aerosol emissions. In addition, the acid solubilization of dust particles (i.e., conversion from mineral P to phosphate) takes place in both aerosol water and cloud droplets, along with the conversion from insoluble to soluble OP aerosols during atmospheric processing. The CTM accounts for two P-containing insoluble minerals

25   (the fluoroapatite and the hydroxyapatite) in dust based on soil mineralogy maps (Nickovic et al., 2012), as well as for OP present in soil's organic matter (Kanakidou et al., 2012). A solubility of 10% is applied to all P-containing dust emissions in the CTM. For P-containing combustion aerosols, the CTM accounts for anthropogenic (i.e., for fossil fuel, coal, waste, and biofuel) and biomass burning emissions, based on observed P/BC mass ratios (Mahowald et al., 2008). Sea-spray and volcanic aerosols account for a rather low DP global source, in contrast to bioaerosols which are estimated to contribute significantly

30   to DOP. The naturally emitted OP by bioaerosols is overall represented by bacteria, fungi, and pollen particles (Myriokefalitakis et al., 2017). More details on the P-cycle representation in the CTM can be found in Myriokefalitakis et al. (2016).

The present-day global annual DIP deposition flux into the global ocean for the CTRL simulation accounts for ~0.10 Tg-P yr^{-1} (Table 1), presenting also a strong spatial variability (Fig. 1h). The highest DIP deposition input rates occur downwind the major dust source regions (~5·10^{-6} kg-P m^{-2} yr^{-1}) owing to the phosphate content in dust emissions. High DIP deposition fluxes (~1·10^{-6} kg-P m^{-2} yr^{-1}) occur downwind heavily forested regions (i.e., Amazonia, Central Africa, and Indonesia) due to

5   the enhanced biomass burning sources. The combustion of anthropogenic origin further contributes to the DIP deposition flux into the ocean, such as downwind the South and East Asia (~1·10^{-6} kg-P m^{-2} yr^{-1}). Notable deposition rates are also illustrated away from dust sources, such as in the Northern Atlantic and Pacific Ocean (~5·10^{-7} kg-P m^{-2} yr^{-1}), due to the mineral P solubilization during atmospheric transport and somewhat lower rates occur in the Southern Ocean. Moreover, consideration of organic fraction in atmospheric DP inputs (Fig. S1e) results in a ~50% increase in the global DP deposition flux (Table 1)

10 and a significant increase of up to 80% can be also seen (Fig. S1f).

An increase in the global DIP deposition of ~40% is considered here for the present-day (i.e., 0.06 Tg-P yr^{-1} for preindustrial conditions) and a modest decrease of ~20% is projected for the year 2100 (i.e., 0.08 Tg-P yr^{-1} under the RCP8.5 scenario), as shown in Table 1. Regional differences for the preindustrial times appear however to be stronger (up to 60 %; Fig. 1g), especially downwind highly populated regions of the Northern Hemisphere, in the Atlantic and Pacific Oceans. DIP deposition

15 fluxes are also projected to decrease over the midlatitudes of the Northern Hemisphere where human activities dominate under the RCP8.5 scenario, with the largest changes up to 40% downwind of China and Australia. Significant changes (~20 %) are also illustrated in the Arabian Sea and the Bay of Bengal due to the expected increases in population (Fig. 1i). Note here that since the CTM neglects any changes in dust and bioaerosol emissions that occurred in the past or are expected in the future, all changes in DP deposition fluxes accounted in PISCES are solely driven by changes in the anthropogenic and biomass

20 burning emissions, along with the changes in insoluble to soluble conversions rates due to atmospheric processing.

3 Results and discussion

3.1 Oceanic nutrient concentrations

Nitrate: The simulated annual mean nitrate surface concentrations in the seawater for the present-day and the relative differences for past and future eras are presented in Fig. 2. The present-day surface nitrate distribution shows high

25 concentrations along the equatorial divergence where nutrients are upwelled, and solar insolation supports good light conditions throughout the year. In the high latitudes, cooler water temperatures and seasonally damped light conditions reduce nutrient consumption by biological productivity, resulting overall in elevated annual mean nutrient concentrations. High surface concentrations are also calculated in the Southern Ocean where the deep convection around Antarctica maintains high nutrient transports to the surface and lowers phytoplankton growth by a thick mixed layer. Elevated nutrient concentrations

30 are likewise simulated in the Eastern Equatorial Pacific, and the Subarctic North Pacific, i.e., the well-known HNLC regions. All in all, this reflects a reasonable simulation of the abiotic oceanographic processes in the model.

Increased atmospheric nitrogen deposition from the preindustrial to the modern era (Table 1) results in a respective increase in surface nitrate concentrations in almost all oceanic regions, with some exceptions in the Eastern Equatorial and the subpolar Pacific Ocean (Fig. 2a). In remote oceanic areas and far from any coastal or riverine nutrient supply (thus also strongly Fe-limited), the higher present-day inorganic nitrogen and iron atmospheric inputs compared to the preindustrial era (Figs. 1a,d)

5   results in an increase in primary production (see also Sect. 3.3). This may, overall, lead to a more efficient export of the surface seawater nitrogen to the deeper ocean in the form of sinking biogenic particles in these oligotrophic oceanic regions (e.g., Krishnamurthy et al., 2007, 2010). For the future conditions, however, the model calculates both negatives and positive changes in the surface nitrate concentrations, resulting from an overall decrease (~4%) of the global inorganic nitrogen oceanic input (from atmospheric deposition and N_2-fixation) (Table 1). Indeed, for the future era, a decrease in almost all oceanic regions is

10 calculated, except for the coastlines of Southeast Asia, Africa, and South America (Fig. 1c).

Figure 3 illustrates the comparison between the simulated present-day surface nitrate concentration and the compiled data from the World Ocean Atlas (WOA; Garcia et al., 2010b) for two seasons: the boreal winter (December, January, and February; DJF) and the boreal summer (June, July, and August; JJA). Generally, the model compares quite well with the nitrate surface observations. However, compared to the WOA compilation (Figs. 3a,b) the modelled nitrate concentrations (Figs. 3c,d,

15 respectively) are lower in the northern high latitudes for both seasons (~5-10 mmol/m^3), especially in the Subpolar Pacific Ocean (up to 30 mmol/m^3) during DJF. This is likely related to the model's too shallow mixed layer thickness (not shown) and as a consequence, the transport of nutrients and from deeper layers to the surface is likewise underestimated during the winter season. On the other hand, the surface nitrate concentrations are somewhat overestimated in the Southern Ocean for both seasons (Figs. 3e,f). This is also the case when the model uses PISCES defaults atmospheric deposition fields and it might

20 be related to deficiencies in the model's abiotic processes. In addition, as also explained by Aumont et al. (2015), the WOA climatology may be biased toward lower values since most of the observational data have been collected during the productive season in that region.

Iron: Figure 2 further presents the annual mean surface concentrations of iron as calculated for present-day in CTRL simulation along with the respective past and future relative differences. Present-day surface iron distribution (Fig. 2e) present high

25 concentrations in the subtropical North Atlantic Ocean and in the Arabian Sea, with the lowest surface concentrations being calculated in the Eastern Equatorial Pacific and in the Southern Ocean. A secondary maximum in iron concentrations is calculated in the Subarctic North Pacific. In general, and as also seen in other modelling studies, iron concentrations in the model are low, especially in the Southern Ocean, the Eastern Equatorial Pacific, and the Subarctic North Pacific, with the highest oceanic concentrations to be calculated along the coasts or over the continental margins. For the past (Fig. 2d) and

30 future (Fig. 2f) conditions, the model calculates in general lower iron surface concentrations, reflecting overall the respective decreases in DFe deposition fluxes into the ocean (Figs. 1d,c, respectively).

Figure 4 presents the comparison of the modelled with observed oceanic iron concentrations in the upper 100m, for two seasons (DJF and JJA). The DFe oceanic observation data (Figs. 4a,b) are taken from Tagliabue et al. (2012) (https://www.bodc.ac.uk/geotraces/data/historical/; last access 29/02/2020). The model simulates reasonably the observed

oceanic iron concentrations for both seasons, for the CTRL simulation (Figs. 4c,d). The observed low oceanic DFe concentrations are well captured in most of the cases by the model, especially for boreal winter (Fig. 4d), but underestimated during boreal summer (Fig. 4d). Low dissolved iron concentrations of about 0.1 nM (i.e., $1nM = 10^{-9}$ moles per liter) are simulated and observed in the subtropical Atlantic and Pacific basins, especially in the HNLC regions. The high observed

5   oceanic DFe concentrations (>1 nM) are also well simulated along the coasts and over the continental margins as a result of sediment mobilization. In the vicinity of intense dust sources, such as the Sahara, the upper ocean in the model is strongly influenced by the atmospheric inputs, and some higher values compared to observations (up to 0.5 nM) are simulated in the North Atlantic Ocean, for both seasons. The model also slightly overestimates the observed DFe concentrations in the North Pacific, as well as in the subpolar Southern Ocean (Pacific sector) during the local summer season. This may be related to the

10 too low consumption of nutrients, as the model may underestimate the biological production in this area (Fig. 7). In the subtropical South Atlantic, the low DFe oceanic concentrations are well captured, although during boreal summer the model slightly underestimates the observations. In the Southern tropical Pacific during boreal summer, the low surface concentrations for the Fe-limited latitudes are also underestimated. Moreover, across the Southern Ocean (except for the subpolar sector) the model calculates lower values for the DFe concentrations.

15 **Phosphate**: The annual mean present-day phosphate surface concentrations as calculated for the CTRL simulation together with the respective relative differences for past and future eras are presented in Figs. 2g-i. In general, the phosphate concentrations show similar distributions as the dissolved inorganic nitrogen. The surface phosphate distribution in the model shows high concentrations along the equatorial divergence where nutrient-rich deep water is upwelled, as well as in the high latitudes, with the highest surface concentrations to be simulated in the Southern Ocean. A secondary maximum is calculated

20 in the Eastern Equatorial Pacific and the Subarctic North Pacific; both regions are subject to large scale oceanic upwelling of deep waters. Note that in general, phosphate concentrations in deep waters are higher than at the surface where nutrients are removed by biotic productivity and exported by sinking particulate organic matter to the deeper ocean. However, due to the constant Redfield Ratio (i.e., C:N:P = 122:16:1) applied in the model (Aumont et al., 2015), the phosphorus cycle is closely related to that of nitrogen, as both are subjected to the same large-scale physical processes and circulation in the ocean. An

25 exception is the N_2-fixation which acts as an additional external source for inorganic nitrate in the model. Although the roughly 1.7 times increase in the phosphate deposition inputs to the ocean from preindustrial to the modern era (Table 1), the preindustrial surface phosphate oceanic concentrations are calculated 20-50% higher in most oceanic regions (Fig. 2g), except for the Southern Ocean where no significant change is calculated. Despite the projected decrease of the global phosphate input (Table 1), higher phosphorus surface oceanic concentrations are also simulated for the future, up to ~20% (Fig. 2i). The main

30 reason for these elevated phosphate concentrations is the decreased primary production almost everywhere (Figs. 6d,f). Indeed, as nitrogen is the limiting factor for phytoplankton in the open ocean, the primary production rates have been lowered according to lower nitrogen deposition rates. Accordingly, less phosphate consumption by phytoplankton growth takes place and this outcompetes the effect of lowered P deposition, leading to relatively higher phosphate concentrations. The effect of the decreased productivity on phosphate concentrations would be, however, even stronger if it was not being partly compensated

by higher N₂-fixation rates. Overall, this points to the marine biogeochemical processes as an essential factor in controlling the phosphorus concentrations at the surface ocean.

Figure 5 further compares the simulated surface phosphate concentration with an observation-based data set from WOA, for the summer and winter seasons. The global pattern of observed phosphate is mainly controlled by the ocean dynamics and it

5   is well reproduced by the model. Hence, during winter enhanced wind mixing and convective mixing transport nutrient-rich deep water to the surface in the North Atlantic and North Pacific. At the same time, nutrient consumption by biological productivity in the high latitudes is weak due to low winter temperatures and reduced light conditions. The resulting maximum phosphate concentrations in the Atlantic and Pacific subpolar gyres, however, are somewhat underestimated (up to 1.5 mmol/m³) by the model compared to the WOA data (Figs. 5a,b). This is also caused by a too shallow winter mixed layer depth

10 simulated by the physical model NEMO as forced by the OMIP standard forcing.

3.2 Nitrogen fixation

For the CTRL simulation, the nitrogen fixation is calculated about 112 Tg-N yr⁻¹ for the present day (Table 1). The respective relative differences compared to past and future periods are also presented in Figs. 6a-c. Compared to modern times, the model calculates a significant decrease (up to 20%) in nitrogen fixation in the tropical and subtropical Pacific and the subtropical

15 Atlantic Ocean for the preindustrial era. On the contrary, downwind land sources such as the Bay of Bengal and Indonesia, nitrogen fixation is higher for the preindustrial conditions, due to the lower nitrogen deposition fluxes accounted by the model (see Sect. 2.2.1). Finally, the nitrogen fixation rates present very low differences in the Equatorial Pacific, Equatorial Atlantic, and the Southern Indian Ocean (0-10%) away from land sources (Fig. 6a). Note, however, that nitrogen fixation in PISCES is restricted only to warm waters (i.e., above 20° C). On a global scale, the model calculates overall only a small increase (0.2%;

20 Table 1) in present-day nitrogen fixation rates compared to preindustrial times, mainly as a result of the increased soluble iron inputs in the subtropical North Pacific (Fig. 1d). For the future conditions, the model also calculates a modest decrease in the global nitrogen fixation (Table 1) with the projected decrease of the global inorganic nitrogen and iron inputs to the ocean (Figs. 1c,f, respectively) to result overall in some lower rates (up to 10%) in the Equatorial Pacific Ocean (Fig. 6c).

3.3 Primary production

25 The present-day annual mean primary production together with the relative differences compared to past and future periods are presented in Figs. 6d-f. The primary production distribution in the open ocean shows high rates along the equatorial divergence and in the high latitudes, where nutrients concentrations are high. The decreased nitrogen deposition during preindustrial conditions compared to present-day results in lowered primary production rates almost in all oceanic regions. On the contrary, a projected modest decrease of primary production rates is calculated by the model (Fig. 6f), owing also to the

30 lower (~14%) dissolved iron deposition fluxes implemented from present to future conditions (Fig. 1f).

A comparison between satellite estimates and model simulations of the global primary production is presented in Fig. 7. The present-day modelled globally integrated production (~47 Pg yr⁻¹) is lower compared to satellite-based estimates from

SeaWiFS (Behrenfeld et al., 2005) obtained equal to ~60-67 Pg yr^{-1}, but in the range of estimates from other studies (e.g., 50.7 ± 9.5 Pg yr^{-1}; Carr et al., 2006). The simulated primary production reproduces the main features derived from satellite-based observations (Behrenfeld et al., 2005). The model simulates relatively low rates (~200 mg-C m^{-2} day^{-1}) in the subtropical gyres and higher rates (> 500 mg-C m^{-2} day^{-1}) in upwelling regions, the North Atlantic and the Southern Ocean. However, as also

5   known from other modeling studies, the primary production in the tropics might be overestimated, whereas in the higher latitudes underestimated (e.g., Steinacher et al., 2010). High productivity in the open ocean areas is linked to upwelling areas such as the equatorial divergence zones or coastal upwellings, like at the west coasts of South Africa or northern South America. Primary productivity rates are underestimated in the North Atlantic region, probably due to the low accumulation of nutrients during winter as already discussed.

10   Figure 7 further illustrates the simulated primary production for the boreal winter (DJF) and summer (JJA), compared to the respective observation-based data. The model generally compares reasonably for both seasons; however, the modelled primary production rates (Figs. 7e,f, respectively) are calculated lower in the high latitudes. The pronounced seasonality due to light limitation and temperature of phytoplankton growth in the North Atlantic is well captured by the model. During the warm season, higher water temperatures and better light conditions increase primary production and the nutrient consumption by

15   phytoplankton growth in the high latitudes. This results in depleted nutrient concentrations in the North Atlantic during boreal summer. In the North Pacific, which is known as an HNLC region, nutrients still remain at higher levels due to insufficient iron support. This is somewhat underestimated in the model as the simulated nitrate concentrations are too low (Fig. 3f), probably related to the slightly high iron concentrations in the upper 100 m North Pacific (Figs. 4d,f). The same biases mentioned for phosphate are likewise seen in the nitrate concentration as most features are mainly controlled by the model

20   physics. Overall, only nitrogen fixation and denitrification can modulate the nitrate concentrations, apart from all other processes that also influence the phosphate in the same way (e.g., productivity, remineralization dissolution, etc.).

3.4 Biogeochemistry responses to atmospheric organic nutrients

The differences of nitrogen fixation and primary production rates between the CTRL and the ORGF simulations are here used to estimate the response of the marine ecosystem to the contribution of the organic fraction in the atmospheric nutrient (N, P,

25   and Fe) inputs. Most biogeochemistry studies account for the inorganic fraction of nutrients as the most important pool on nitrogen from the atmospheric pathway. On the contrary, uncertainty still exists with respect to the organic fraction in atmospheric fluxes into the ocean. However state-of-the-art atmospheric chemistry models can nowadays efficiently calculate the total dissolved nutrient atmospheric deposition fluxes including the organic part, which seems to be overall rather important for the total magnitude of the atmospheric input to the ocean (see Fig. S1). To investigate the role of organic components, we

30   separated the inorganic and organic fractions of the atmospheric nutrients to isolate their contributions to the marine biogeochemistry. Note that our approach is supported by the fact that PISCES, as also other biogeochemistry models, does not separately model the dissolved organic nitrogen (DON) and phosphorus (DOP), but all the dissolved organic matter is assumed to be instantaneously remineralized to the respective inorganic pools, i.e., the DIN and the DIP (see Aumont et al., 2015).

When the organic fraction of the atmospheric nutrients is considered in the model, a modest decrease in nitrogen fixation of ~0.5 Tg-N yr^{-1} is calculated for present-day conditions (Table 1). The increased soluble Fe inputs (~25%) relative to the CTRL simulations - although smaller compared to relative increases of N (~45%) and P (~50%) - tend to reduce the Fe-limitation in diazotrophs. Thus, the reduced Fe- and P- limitations along with the extra atmospheric inputs of ON to the ocean, overall

5   decrease the global nitrogen fixation rates in the model (Fig. 8a). Note, however, that the nitrogen fixation is a rather energy-expensive process that is known to be inhibited in the excess of ammonium, in particular. Thus, the assumption of a rapid DON remineralization, considering also that the ON in the atmospheric particulate phase predominantly contains reduced nitrogen, may lead partially to an overestimation of the response of nitrogen fixation rates when accounting for the organic fraction of atmospheric nutrients.

10   Compared to CTRL, the nitrogen fixation rates for the ORGF simulation are significantly more intense (up to ~90%) in the tropical Pacific Ocean but suppressed (up to ~40%) in the tropical Atlantic Ocean (Fig. 8b). Especially in the Indonesian throughflow and in the eastern tropical Atlantic along central Africa, significantly reduced rates (more than 90%) are calculated for the ORGF simulation. The suppressed nitrogen fixation rates are mainly calculated due to the additional ON deposition in the ocean. Nitrogen fixation is also decreased in the tropical Atlantic Ocean for the ORGF simulation. However, increased

15   soluble Fe inputs to the tropical Pacific (Fig. S1d) for the ORGF simulation, partially decreased the Fe limitation of diazotrophs and increase nitrogen fixation in these remote oceanic regions. Overall, compared to CTRL, the simulated global nitrogen fixation for the ORGF simulation leads to a net decrease by only ~0.4% (Table 1), although pronounced regional differences between the two simulations exist (Fig. 8b).

In contrast to the rather balanced nitrogen fixation rates, the primary production rates increased in the ORGF simulation (Fig.

20   8c), as the total atmospheric nitrogen inputs increased in the model (Fig. S1). According to global calculations, the primary production increased from ~46.7 Pg-C yr^{-1} for the CTRL to ~47.8 Pg-C yr^{-1} for the ORGF (Table 1). This increase may correspond to a modest decline of atmospheric pCO$_2$ of ~1.3 ppm, solely when accounting the organic fraction in atmospheric inputs in the model. The respective percentage differences compared to the CTRL simulation are presented in Fig. 8d. Primary production increases almost in all ocean basins (except some parts of the Subpolar Pacific Ocean) for the ORGF simulation.

25   Moreover, higher rates are calculated in the Subpolar Atlantic Ocean (up to 15 %). In the N-limited oceanic regions, the increased ORGF atmospheric nitrogen deposition (Fig. S1b) directly increases the production rates (Fig. 8d). In the western subtropical North Pacific, the atmospheric N deposition supported an extra production up to 15%. The production rates are also increased in the open subtropical South Pacific and Atlantic Oceans up to nearly 20% in the ORGF simulation.

4 Summary and conclusions

The atmospheric deposition of natural and anthropogenic gases and aerosols to the ocean's surface supply essential nutrients that impact phytoplankton and hence the primary production. Recent advancements in atmospheric chemistry and transport dynamics have resulted in new scenarios for the atmospheric pathways of substances relevant to marine biogeochemistry. The effect of these scenarios, however, can be hardly tested in state-of-the-art ESMs, as this would be extremely expensive due to the high demands of computational power. Thus, a working approach to estimate the effect of these scenarios to the marine biogeochemistry is in offline modus, by forcing the individual Earth system components with the revised deposition data. For this work, we applied the marine carbon cycle and biogeochemistry model PISCES, as part of the ESM EC-Earth, to study the effect of state-of-the-art global atmospheric deposition estimates of nitrogen, iron, and phosphorus on the oceanic productivity. The global patterns of modeled nutrient concentrations are here realistically simulated compared to climatological and observational data. The variability of primary production in space and time is also well in the range of satellite-based estimates and modelled published values. The nutrient-depleted subtropical gyres are likewise reproduced, as well as, the local enhanced nutrient concentrations as associated with the equatorial divergence zone. Note that as PISCES was here run in forced mode, the too shallow oceanic mixed layer that resulted from a too weak salinity restoring, caused the high northern latitudes to be too fresh in the upper water column, imposing thus a negative feedback on mixing. However, the weak salinity restoring was chosen as a compromise to maintain an acceptable deep convection in the Labrador Sea and Irminger Sea. On the other hand, the salinity restoring should not be too strong, as the OMIP simulation has been prolonged to test the model's sensitivity to climate warming. For this, the initialization files of the final OMIP year were used and the model was further forced with bias-corrected forcing from the RCP8.5 scenario taken from the previous CMIP5 run of the EC-Earth consortium. Nevertheless, for the prolongation run, it was essential not to restrict the model close to the present-day salinity fields.

For the present day, ~40 Tg-N yr^{-1}, ~0.28 Tg-Fe yr^{-1} and ~0.10 Tg-P yr^{-1} of nitrogen, iron, and phosphorus atmospheric inputs to the global ocean, accounting for only their inorganic fractions, were considered in PISCES. This resulted in a global nitrogen-fixation rate of ~112 Tg-N yr^{-1} and an integrated primary production of roughly 47 Pg-C yr^{-1}. Compared to present-day conditions, the lower preindustrial atmospheric nutrient inputs to the ocean result in a weakened primary production of ~2% globally. This decrease in oceanic productivity was supported in the model by the preindustrial decrease in soluble iron inputs (combustion sources and atmospheric processing of mineral aerosols) along with the substantial decrease in atmospheric anthropogenic nitrogen inputs. The projected changes in air pollutants under the RCP8.5 emission scenario resulted in a modest decrease in marine productivity compared to modern times, overall returning the calculated primary production rates to almost the preindustrial levels. Global nitrogen-fixation rates also presented a marginal variability, although some notable decreases were calculated for the modern subtropical Pacific and Atlantic gyres.

Another feature tested in the present study is the contribution of organics to the atmospheric inputs to the global ocean. On a global scale, the effect of the atmospheric organic nutrient deposition fluxes on the primary production was modest, i.e., a ~2% increase in present-day primary production. This increase was almost equal to the response of the increased emissions and

atmospheric processing on the oceanic biogeochemistry since preindustrial times in the model when only the inorganic fraction is considered. However, as organic nutrients generally increased the deposition fluxes, some stronger changes in the oceanic productivity were calculated in the oligotrophic subtropical gyres, becoming overall less nutrient-stressed.

PISCES was here driven by physical outputs from the ocean model NEMO, forced by present-day climate conditions as provided by OMIP. Therefore, the presented experiments did not account for the impact of future climate change which could interact or may even mask the effect of changed deposition considered here. Consequently, the here found effects are subject to some uncertainties related to the potential interaction with climate change. Furthermore, climate-induced changes in the global wind system may not only alter atmospheric pathways for nutrients but also impact on oceanic up- and down-welling. Thus, shifts in the seasonal position of trade winds will likewise force shifts in the position of open-ocean and coastal upwelling. These regions are usually nutrient-rich and not particularly sensitive to varying atmospheric nutrient inputs. Displacements of these upwelling positions as a result of climate change can increase the sensitivity to external nutrient inputs in regions formerly impacted by upwelling. On the other hand, several studies have demonstrated that mid to high latitude areas, such as the North Atlantic and the Arctic, will be more stratified in a future warmer climate (Fu et al., 2016; Gröger et al., 2013; Steinacher et al., 2010) with negative feedback on vertical mixing and marine primary production due to reduce upward transport of nutrient into the photic zone. Accordingly, primary production in these regions will probably be more sensitive to changed atmospheric deposition rates in the future climate.

Our results imply only marginal effects in cold regions like the Arctic Ocean. This is certainly robust under the present climate when marine productivity is limited by temperature and sea-ice reducing light conditions in these regions. However, there is a large agreement that climate change is most severe in the high latitudes, with strong increases in the water temperatures and substantially diminished sea ice cover in the Arctic. Thus, temperature and light limitation will likely become less important in a future climate in this region and thus, nutrient limitations will increase. Consequently, changes in atmospheric transport and deposition of the bioavailable nutrients may play a larger role in the future climate than today, especially under the high-emission climate scenarios such as RCP8.5. An example can be seen in the high latitude Southern Ocean around Antarctica where the major amount of surplus DFe is deposited in our PAST and FUTURE experiments. As expected, the additional DFe availability had nearly no effect on productivity as convective mixing and extremely cold water temperatures maintained sufficient nutrients and support low productivity under the present-day climate. This may, however, change with altered oceanographic conditions under a future warmer climate. In the northwestern Pacific, known as an HNLC region where iron is the limiting factor, the increased supply of DFe clearly stimulated marine productivity in the FUTURE experiment. This increase in productivity is likely underestimated because our experiments lacked the climate-induced changes in stratification which would reduce the nutrient supply from the deep ocean. Note also that although several studies suggest that dust fluxes may be sensitive to climate change and the land use changes (e.g., Ginoux et al., 2012; Mahowald et al., 2010; Prospero and Lamb, 2003), and thus could be an important driver of the atmospheric nutrient cycles, for this study the atmospheric CTM did not account for any changes in dust emissions for the preindustrial and future conditions, but they were kept constant to the present-day atmosphere (i.e., the year 2010).

The combined effect of climate change and atmospheric deposition is beyond the scope of the present study. However, this work asserts the importance of an explicit representation of the atmospheric nutrients in the context of biogeochemistry modeling, providing also a first assessment of the contribution of another source of atmospheric nutrients than inorganics, i.e., the organic nutrients, and their potential impact on the oceanic productivity. Finally, despite the here discussed effects on

5   nutrient-depleted ocean regions, the global ocean turned out to be notably robust with regard to the oceanic productivity, against realistic scenarios for future and past atmospheric nutrient supply. The same conclusions can likely be reached by other biogeochemistry models. This might be related to the large part of newly produced particular organic matter that is already remineralized within the ocean's mixed layer, so that nutrients formerly incorporated in the soft tissue becomes again rapidly bioavailable. Remineralization in state-of-the-art models, however, is parameterized according to present-day empirical

10   relationships, as well as the models' biogeochemistry and ocean dynamics are tuned against climatologies valid for the present-day climate. Furthermore, a more explicit representation of the nutrients' stoichiometric variability, rather than the fixed Redfield ratios routinely used in global biogeochemistry models, will allow a better representation of the marine productivity in protected climate forcings. Further investigations of the impact of the atmospheric nutrient inputs to the global oceanic productivity are required under available climate change scenarios for the physical ocean and accounting for variable Redfield

15   ratios in the marine environment.

Author contribution: SM prepared the atmospheric input fields, preformed the simulations and the model evaluation. MG prepared the model initialization fields. All authors contributed to the manuscript preparation.

Acknowledgments: Stelios Myriokefalitakis acknowledges financial support for this research from the European Union's
5 Horizon 2020 research and innovation programme under the Marie Skłodowska-Curie grant agreement no. 705652 – ODEON. Matthias Gröger and Jenny Hieronymus acknowledges support from the European Commission's Horizon 2020 Framework Programme, under Grant Agreement number 641816, the "Coordinated Research in Earth Systems and Climate: Experiments, kNowledge, Dissemination and Outreach (CRESCENDO)". Stelios Myriokefalitakis acknowledges support from the Joint Group of Experts on the Scientific Aspects of Marine Environmental Protection (GESAMP; http://www.gesamp.org/),
10 Working Group 38, the Atmospheric Input of Chemicals to the Ocean. The authors thank Alessandro Tagliabue for providing the dissolved iron oceanic concentration dataset. Model simulations were carried out on the Bi cluster operated by the Swedish National Supercomputer Centre (http://www.nsc.liu.se/) and data processing supported by computational time granted by the Greek Research and Technology Network (GRNET) in the National HPC facility ARIS (https://hpc.grnet.gr/), under project PR006002-ADIOS. The publication of this work was financed by the internal grant programme of the National Observatory
15 of Athens "Atmospheric deposition impacts on the ocean system" (number 5065).

Competing interests: The authors declare that they have no conflict of interest.

References

Aumont, O. and Bopp, L.: Globalizing results from ocean in situ iron fertilization studies, Global Biogeochem. Cycles, 20(2), GB2017, doi:10.1029/2005GB002591, 2006.

Aumont, O., Ethé, C., Tagliabue, A., Bopp, L. and Gehlen, M.: PISCES-v2: an ocean biogeochemical model for carbon and
5 ecosystem studies, Geosci. Model Dev., 8(8), 2465–2513, doi:10.5194/gmd-8-2465-2015, 2015.

Barkley, A. E., Prospero, J. M., Mahowald, N., Hamilton, D. S., Popendorf, K. J., Oehlert, A. M., Pourmand, A., Gatineau, A., Panechou-Pulcherie, K., Blackwelder, P. and Gaston, C. J.: African biomass burning is a substantial source of phosphorus deposition to the Amazon, Tropical Atlantic Ocean, and Southern Ocean, Proc. Natl. Acad. Sci. U. S. A., 116(33), 16216–16221, doi:10.1073/pnas.1906091116, 2019.

10 Behrenfeld, M. J., Boss, E., Siegel, D. A. and Shea, D. M.: Carbon-based ocean productivity and phytoplankton physiology from space, Global Biogeochem. Cycles, 19(1), 1–14, doi:10.1029/2004GB002299, 2005.

Behrenfeld, M. J., O'Malley, R. T., Siegel, D. A., McClain, C. R., Sarmiento, J. L., Feldman, G. C., Milligan, A. J., Falkowski, P. G., Letelier, R. M. and Boss, E. S.: Climate-driven trends in contemporary ocean productivity, Nature, 444(7120), 752–755, doi:10.1038/nature05317, 2006.

15 Camarero, L. and Catalan, J.: Atmospheric phosphorus deposition may cause lakes to revert from phosphorus limitation back to nitrogen limitation, Nat. Commun., 3, 1118, doi:10.1038/ncomms2125, 2012.

Carr, M.-E., Friedrichs, M. A. M., Schmeltz, M., Noguchi Aita, M., Antoine, D., Arrigo, K. R., Asanuma, I., Aumont, O., Barber, R., Behrenfeld, M., Bidigare, R., Buitenhuis, E. T., Campbell, J., Ciotti, A., Dierssen, H., Dowell, M., Dunne, J., Esaias, W., Gentili, B., Gregg, W., Groom, S., Hoepffner, N., Ishizaka, J., Kameda, T., Le Quéré, C., Lohrenz, S., Marra, J.,
20 Mélin, F., Moore, K., Morel, A., Reddy, T. E., Ryan, J., Scardi, M., Smyth, T., Turpie, K., Tilstone, G., Waters, K. and Yamanaka, Y.: A comparison of global estimates of marine primary production from ocean color, Deep Sea Res. Part II Top. Stud. Oceanogr., 53(5–7), 741–770, doi:10.1016/j.dsr2.2006.01.028, 2006.

Dee, D. P., Uppala, S. M., Simmons, A. J., Berrisford, P., Poli, P., Kobayashi, S., Andrae, U., Balmaseda, M. A., Balsamo, G., Bauer, P., Bechtold, P., Beljaars, A. C. M., van de Berg, L., Bidlot, J., Bormann, N., Delsol, C., Dragani, R., Fuentes, M.,
25 Geer, A. J., Haimberger, L., Healy, S. B., Hersbach, H., Hólm, E. V, Isaksen, L., Kållberg, P., Köhler, M., Matricardi, M., McNally, A. P., Monge-Sanz, B. M., Morcrette, J.-J., Park, B.-K., Peubey, C., de Rosnay, P., Tavolato, C., Thépaut, J.-N., Vitart, F., Berg, L. Van De, Bidlot, J., Bormann, N., Delsol, C., Dragani, R., Fuentes, M., Geer, A. J. and Dee, D. P.: The ERA-Interim reanalysis: configuration and performance of the data assimilation system, Q. J. R. Meteorol. Soc., 137(656), 553–597, doi:10.1002/qj.828, 2011.

30 Duce, R. A., Liss, P. S., Merrill, J. T., Atlas, E. L., Hicks, B. B., Millertl, J. M., Prospero, J. M., Arimoto, R., Church, T. M., Ellis, W., Galloway, J. N., Hansen, L., Knap, A. H., Reinhardt, K. H., Soudine, A., Tsunogai, S., Wollast, R. and Zhou, M.: The atmospheric input of trace species to the world ocean, Global Biogeochem. Cycles, 5(3), 193–259, 1991.

Duce, R. A., LaRoche, J., Altieri, K., Arrigo, K. R., Baker, A. . R., Capone, D. G., Cornell, S., Dentener, F., Galloway, J.,

Ganeshram, R. S., Geider, R. J., Jickells, T. D., Kuypers, M. M., Langlois, R., Liss, P. S., Liu, S. M., Middelburg, J. J., Moore, C. M., Nickovic, S., Oschlies, A., Pedersen, T., Prospero, J., Schlitzer, R., Seitzinger, S., Sorensen, L. L., Uematsu, M., Ulloa, O., Voss, M., Ward, B. and Zamora, L.: Impacts of Atmospheric Anthropogenic Nitrogen on the Open Ocean, Science (80-.)., 320(5878), 893–897, doi:10.1126/science.1150369, 2008.

5   Falkowski, P. G., Scholes, R. J., Boyle, E., Canadell, J., Canfield, D., Elser, J., Gruber, N., Hibbard, K., Högberg, P., Linder, S., Mackenzie, F. T., Moore, B., Pedersen, T., Rosenthal, Y., Seitzinger, S., Smetacek, V. and Steffen, W.: The Global Carbon Cycle: A Test of Our Knowledge of Earth as a System, Science (80-.)., 290(5490), 291–296, doi:10.1126/science.290.5490.291, 2000.

Fountoukis, C. and Nenes, A.: ISORROPIA II: a computationally efficient thermodynamic equilibrium model for K+–Ca2+–
10 Mg2+–NH4+–Na+–SO42−–NO3, Atmos. Chem. Phys., 7(17), 4639–4659, doi:10.5194/acp-7-4639-2007, 2007.

Fu, W., Randerson, J. T. and Moore, J. K.: Climate change impacts on net primary production (NPP) and export production (EP) regulated by increasing stratification and phytoplankton community structure in the CMIP5 models, Biogeosciences, 13(18), 5151–5170, doi:10.5194/bg-13-5151-2016, 2016.

Garcia, H., Locarnini, R., Boyer, T., Antonov, T., Baranova, O., Zweng, M. and Johnson, D.: WORLD OCEAN ATLAS 2009
15 Volume 3: Dissolved Oxygen, Apparent Oxygen Utilization, and Oxygen Saturation, U.S. Government Printing Office, Washington DC., 2010a.

Garcia, H. E., Locarnini, R. A., Boyer, T. P., Antonov, J. I., Zweng, M. M., Baranova, O. K. and Johnson, D. R.: WORLD OCEAN ATLAS 2009 Volume 4: Nutrients (phosphate, nitrate and silicate), U.S. Government Printing Office, Washington, D.C., 2010b.

20 Ginoux, P., Prospero, J. M., Gill, T. E., Hsu, N. C. and Zhao, M.: Global-scale attribution of anthropogenic and natural dust sources and their emission rates based on MODIS Deep Blue aerosol products, Rev. Geophys., 50(3), RG3005, doi:10.1029/2012RG000388, 2012.

Gröger, M., Maier-Reimer, E., Mikolajewicz, U., Moll, A. and Sein, D.: NW European shelf under climate warming: implications for open ocean – shelf exchange, primary production, and carbon absorption, Biogeosciences, 10(6),
25 3767–3792, doi:10.5194/bg-10-3767-2013, 2013.

Gruber, N.: The Dynamics of the Marine Nitrogen Cycle and its Influence on Atmospheric CO2 Variations, in The Ocean Carbon Cycle and Climate, pp. 97–148, Springer Netherlands, Dordrecht., 2004.

Gruber, N., Gloor, M., Mikaloff Fletcher, S. E., Doney, S. C., Dutkiewicz, S., Follows, M. J., Gerber, M., Jacobson, A. R., Joos, F., Lindsay, K., Menemenlis, D., Mouchet, A., Müller, S. A., Sarmiento, J. L. and Takahashi, T.: Oceanic sources, sinks,
30 and transport of atmospheric CO2, Global Biogeochem. Cycles, 23(1), GB1005, doi:10.1029/2008GB003349, 2009.

Guieu, C., Dulac, F., Ridame, C. and Pondaven, P.: Introduction to project DUNE, a DUst experiment in a low Nutrient, low chlorophyll Ecosystem, Biogeosciences, 11(2), 425–442, doi:10.5194/bg-11-425-2014, 2014.

Hajima, T., Watanabe, M., Yamamoto, A., Tatebe, H., Noguchi, A., Abe, M., Ohgaito, R., Ito, A., Yamazaki, D., Okajima, H., Ito, A., Takata, K., Ogochi, K., Watanabe, S. and Kawamiya, M.: Description of the MIROC-ES2L Earth system model and

evaluation of its climate-biogeochemical processes and feedbacks, Geosci. Model Dev. Discuss, doi:10.5194/gmd-2019-275, 2019.

Huneeus, N., Schulz, M., Balkanski, Y., Griesfeller, J., Prospero, J., Kinne, S., Bauer, S., Boucher, O., Chin, M., Dentener, F., Diehl, T., Easter, R., Fillmore, D., Ghan, S., Ginoux, P., Grini, A., Horowitz, L., Koch, D., Krol, M. C., Landing, W., Liu, X.,

5   Mahowald, N., Miller, R., Morcrette, J.-J., Myhre, G., Penner, J., Perlwitz, J., Stier, P., Takemura, T. and Zender, C. S.: Global dust model intercomparison in AeroCom phase I, Atmos. Chem. Phys., 11(15), 7781–7816, doi:10.5194/acp-11-7781-2011, 2011.

Ito, A.: Global modeling study of potentially bioavailable iron input from shipboard aerosol sources to the ocean, Global Biogeochem. Cycles, 27(1), 1–10, doi:10.1029/2012GB004378, 2013.

10   Ito, A. and Xu, L.: Response of acid mobilization of iron-containing mineral dust to improvement of air quality projected in the future, Atmos. Chem. Phys., 14(7), 3441–3459, doi:10.5194/acp-14-3441-2014, 2014.

Ito, A., Myriokefalitakis, S., Kanakidou, M., Mahowald, N. M., Scanza, R. A., Hamilton, D. S., Baker, A. R., Jickells, T., Sarin, M., Bikkina, S., Gao, Y., Shelley, R. U., Buck, C. S., Landing, W. M., Bowie, A. R., Perron, M. M. G., Guieu, C., Meskhidze, N., Johnson, M. S., Feng, Y., Kok, J. F., Nenes, A. and Duce, R. A.: Pyrogenic iron: The missing link to high iron

15   solubility in aerosols, Sci. Adv., 5(5), eaau7671, doi:10.1126/sciadv.aau7671, 2019a.

Ito, A., Ye, Y., Yamamoto, A., Watanabe, M. and Aita, M. N.: Responses of ocean biogeochemistry to atmospheric supply of lithogenic and pyrogenic iron-containing aerosols, Geol. Mag., 1–16, doi:10.1017/S0016756819001080, 2019b.

Kanakidou, M., Duce, R. A., Prospero, J. M., Baker, A. R., Benitez-Nelson, C., Dentener, F. J., Hunter, K. A., Liss, P. S., Mahowald, N., Okin, G. S., Sarin, M., Tsigaridis, K., Uematsu, M., Zamora, L. M. and Zhu, T.: Atmospheric fluxes of organic

20   N and P to the global ocean, Global Biogeochem. Cycles, 26(3), 2011GB004277, doi:10.1029/2011GB004277, 2012.

Kanakidou, M., Myriokefalitakis, S., Daskalakis, N., Fanourgakis, G., Nenes, A., Baker, A. R., Tsigaridis, K. and Mihalopoulos, N.: Past, Present, and Future Atmospheric Nitrogen Deposition, J. Atmos. Sci., 73(5), 2039–2047, doi:10.1175/JAS-D-15-0278.1, 2016.

Kanakidou, M., Myriokefalitakis, S. and Tsigaridis, K.: Aerosols in atmospheric chemistry and biogeochemical cycles of

25   nutrients, Environ. Res. Lett., 13(6), 063004, doi:10.1088/1748-9326/aabcdb, 2018.

Kanakidou, M., Myriokefalitakis, S. and Tsagkaraki, M.: Atmospheric inputs of nutrients to the Mediterranean Sea, Deep Sea Res. Part II Top. Stud. Oceanogr., 171, 104606, doi:10.1016/j.dsr2.2019.06.014, 2020.

Key, R. M., Kozyr, A., Sabine, C. L., Lee, K., Wanninkhof, R., Bullister, J. L., Feely, R. A., Millero, F. J., Mordy, C. and Peng, T.-H.: A global ocean carbon climatology: Results from Global Data Analysis Project (GLODAP), Global Biogeochem.

30   Cycles, 18(4), GB4031, doi:10.1029/2004GB002247, 2004.

Krishnamurthy, A., Moore, J. K., Zender, C. S. and Luo, C.: Effects of atmospheric inorganic nitrogen deposition on ocean biogeochemistry, J. Geophys. Res., 112(G2), G02019, doi:10.1029/2006JG000334, 2007.

Krishnamurthy, A., Moore, J. K., Mahowald, N., Luo, C., Doney, S. C., Lindsay, K. and Zender, C. S.: Impacts of increasing anthropogenic soluble iron and nitrogen deposition on ocean biogeochemistry, Global Biogeochem. Cycles, 23(3), GB3016,

doi:10.1029/2008GB003440, 2009.

Krishnamurthy, A., Moore, J. K., Mahowald, N., Luo, C. and Zender, C. S.: Impacts of atmospheric nutrient inputs on marine biogeochemistry, J. Geophys. Res., 115(G1), G01006, doi:10.1029/2009JG001115, 2010.

Lamarque, J.-F., Shindell, D. T., Josse, B., Young, P. J., Cionni, I., Eyring, V., Bergmann, D., Cameron-Smith, P., Collins, W.
5 J., Doherty, R., Dalsoren, S., Faluvegi, G., Folberth, G., Ghan, S. J., Horowitz, L. W., Lee, Y. H., MacKenzie, I. A., Nagashima, T., Naik, V., Plummer, D., Righi, M., Rumbold, S. T., Schulz, M., Skeie, R. B., Stevenson, D. S., Strode, S., Sudo, K., Szopa, S., Voulgarakis, A. and Zeng, G.: The Atmospheric Chemistry and Climate Model Intercomparison Project (ACCMIP): overview and description of models, simulations and climate diagnostics, Geosci. Model Dev., 6(1), 179–206, doi:10.5194/gmd-6-179-2013, 2013.

10 Laufkötter, C., Vogt, M., Gruber, N., Aumont, O., Bopp, L., Doney, S. C., Dunne, J. P., Hauck, J., John, J. G., Lima, I. D., Seferian, R. and Völker, C.: Projected decreases in future marine export production: the role of the carbon flux through the upper ocean ecosystem, Biogeosciences, 13(13), 4023–4047, doi:10.5194/bg-13-4023-2016, 2016.

Luo, C., Mahowald, N., Bond, T., Chuang, P. Y., Artaxo, P., Siefert, R., Chen, Y. and Schauer, J.: Combustion iron distribution and deposition, Global Biogeochem. Cycles, 22(1), GB1012, doi:10.1029/2007GB002964, 2008.

15 Mahowald, N.: Aerosol Indirect Effect on Biogeochemical Cycles and Climate, Science (80-.)., 334(6057), 794–796, doi:10.1126/science.1207374, 2011.

Mahowald, N., Jickells, T. D., Baker, A. R., Artaxo, P., Benitez-Nelson, C. R., Bergametti, G., Bond, T. C., Chen, Y., Cohen, D. D., Herut, B., Kubilay, N., Losno, R., Luo, C., Maenhaut, W., McGee, K. A., Okin, G. S., Siefert, R. L. and Tsukuda, S.: Global distribution of atmospheric phosphorus sources, concentrations and deposition rates, and anthropogenic impacts,
20 Global Biogeochem. Cycles, 22(4), GB4026, doi:10.1029/2008GB003240, 2008.

Mahowald, N. M., Engelstaedter, S., Luo, C., Sealy, A., Artaxo, P., Benitez-Nelson, C., Bonnet, S., Chen, Y., Chuang, P. Y., Cohen, D. D., Dulac, F., Herut, B., Johansen, A. M., Kubilay, N., Losno, R., Maenhaut, W., Paytan, A., Prospero, J. M., Shank, L. M. and Siefert, R. L.: Atmospheric iron deposition: global distribution, variability, and human perturbations., Ann. Rev. Mar. Sci., 1, 245–278, doi:10.1146/annurev.marine.010908.163727, 2009.

25 Mahowald, N. M., Kloster, S., Engelstaedter, S., Moore, J. K., Mukhopadhyay, S., McConnell, J. R., Albani, S., Doney, S. C., Bhattacharya, A., Curran, M. a J., Flanner, M. G., Hoffman, F. M., Lawrence, D. M., Lindsay, K., Mayewski, P. a., Neff, J., Rothenberg, D., Thomas, E., Thornton, P. E. and Zender, C. S.: Observed 20th century desert dust variability: impact on climate and biogeochemistry, Atmos. Chem. Phys., 10(22), 10875–10893, doi:10.5194/acp-10-10875-2010, 2010.

Mahowald, N. M., Scanza, R., Brahney, J., Goodale, C. L., Hess, P. G., Moore, J. K. and Neff, J.: Aerosol Deposition Impacts
30 on Land and Ocean Carbon Cycles, Curr. Clim. Chang. Reports, 1–16, doi:10.1007/s40641-017-0056-z, 2017.

Matsui, H., Mahowald, N. M., Moteki, N., Hamilton, D. S., Ohata, S., Yoshida, A., Koike, M., Scanza, R. A. and Flanner, M. G.: Anthropogenic combustion iron as a complex climate forcer, Nat. Commun., 9(1), 1593, doi:10.1038/s41467-018-03997-0, 2018.

Meskhidze, N., Völker, C., Al-Abadleh, H. A., Barbeau, K., Bressac, M., Buck, C., Bundy, R. M., Croot, P., Feng, Y., Ito, A.,

Johansen, A. M., Landing, W. M., Mao, J., Myriokefalitakis, S., Ohnemus, D., Pasquier, B. and Ye, Y.: Perspective on identifying and characterizing the processes controlling iron speciation and residence time at the atmosphere-ocean interface, Mar. Chem., 217, 103704, doi:10.1016/j.marchem.2019.103704, 2019.

Moore, C. M., Mills, M. M., Arrigo, K. R., Berman-Frank, I., Bopp, L., Boyd, P. W., Galbraith, E. D., Geider, R. J., Guieu, C., Jaccard, S. L., Jickells, T. D., La Roche, J., Lenton, T. M., Mahowald, N. M., Marañón, E., Marinov, I., Moore, J. K., Nakatsuka, T., Oschlies, A., Saito, M. A., Thingstad, T. F., Tsuda, A. and Ulloa, O.: Processes and patterns of oceanic nutrient limitation, Nat. Geosci., 6(9), 701–710, doi:10.1038/ngeo1765, 2013a.

Moore, J. K. and Doney, S. C.: Iron availability limits the ocean nitrogen inventory stabilizing feedbacks between marine denitrification and nitrogen fixation, Global Biogeochem. Cycles, 21(2), GB2001, doi:10.1029/2006GB002762, 2007.

Moore, J. K., Doney, S. C., Glover, D. M. and Fung, I. Y.: Iron cycling and nutrient-limitation patterns in surface waters of the World Ocean, Deep Sea Res. Part II Top. Stud. Oceanogr., 49(1–3), 463–507, doi:10.1016/S0967-0645(01)00109-6, 2001.

Moore, J. K., Lindsay, K., Doney, S. C., Long, M. C. and Misumi, K.: Marine Ecosystem Dynamics and Biogeochemical Cycling in the Community Earth System Model [CESM1(BGC)]: Comparison of the 1990s with the 2090s under the RCP4.5 and RCP8.5 Scenarios, J. Clim., 26(23), 9291–9312, doi:10.1175/JCLI-D-12-00566.1, 2013b.

Myriokefalitakis, S., Vignati, E., Tsigaridis, K., Papadimas, C., Sciare, J., Mihalopoulos, N., Facchini, M. C., Rinaldi, M., Dentener, F. J., Ceburnis, D., Hatzianastasiou, N., O'Dowd, C. D., van Weele, M. and Kanakidou, M.: Global Modeling of the Oceanic Source of Organic Aerosols, Adv. Meteorol., 2010, 1–16, doi:10.1155/2010/939171, 2010.

Myriokefalitakis, S., Tsigaridis, K., Mihalopoulos, N., Sciare, J., Nenes, A., Kawamura, K., Segers, A. and Kanakidou, M.: In-cloud oxalate formation in the global troposphere: a 3-D modeling study, Atmos. Chem. Phys., 11(12), 5761–5782, doi:10.5194/acp-11-5761-2011, 2011.

Myriokefalitakis, S., Daskalakis, N., Mihalopoulos, N., Baker, A. R., Nenes, A. and Kanakidou, M.: Changes in dissolved iron deposition to the oceans driven by human activity: a 3-D global modelling study, Biogeosciences, 12(13), 3973–3992, doi:10.5194/bg-12-3973-2015, 2015.

Myriokefalitakis, S., Nenes, A., Baker, A. R. A. R., Mihalopoulos, N. and Kanakidou, M.: Bioavailable atmospheric phosphorous supply to the global ocean: a 3-D global modeling study, Biogeosciences, 13(24), 6519–6543, doi:10.5194/bg-13-6519-2016, 2016.

Myriokefalitakis, S., Fanourgakis, G. and Kanakidou, M.: The Contribution of Bioaerosols to the Organic Carbon Budget of the Atmosphere, in Perspectives on Atmospheric Sciences, edited by T. Karacostas, A. Bais, and P. T. Nastos, pp. 845–851, Springer International Publishing., 2017.

Myriokefalitakis, S., Ito, A., Kanakidou, M., Nenes, A., Krol, M. C., Mahowald, N. M., Scanza, R. A., Hamilton, D. S., Johnson, M. S., Meskhidze, N., Kok, J. F., Guieu, C., Baker, A. R., Jickells, T. D., Sarin, M. M., Bikkina, S., Shelley, R., Bowie, A., Perron, M. M. G. and Duce, R. A.: Reviews and syntheses: the GESAMP atmospheric iron deposition model intercomparison study, Biogeosciences, 15(21), 6659–6684, doi:10.5194/bg-15-6659-2018, 2018.

Nenes, A., Krom, M. D., Mihalopoulos, N., Van Cappellen, P., Shi, Z., Bougiatioti, A., Zarmpas, P. and Herut, B.: Atmospheric

acidification of mineral aerosols: A source of bioavailable phosphorus for the oceans, Atmos. Chem. Phys., 11(13), 6265–6272, doi:10.5194/acp-11-6265-2011, 2011.

Nickovic, S., Vukovic, A., Vujadinovic, M., Djurdjevic, V. and Pejanovic, G.: Technical Note: High-resolution mineralogical database of dust-productive soils for atmospheric dust modeling, Atmos. Chem. Phys., 12(2), 845–855, doi:10.5194/acp-12-
5   845-2012, 2012.

Okin, G. S. G. S., Baker, A. R. A. R., Tegen, I., Mahowald, N. M. N. M., Dentener, F. J. F. J., Duce, R. A. R. A., Galloway, J. N. J. N., Hunter, K., Kanakidou, M., Kubilay, N., Prospero, J. M. J. M., Sarin, M., Surapipith, V., Uematsu, M. and Zhu, T.: Impacts of atmospheric nutrient deposition on marine productivity: Roles of nitrogen, phosphorus, and iron, Global Biogeochem. Cycles, 25(2), GB2022, doi:10.1029/2010GB003858, 2011.

10 Orr, J. C., Najjar, R. G., Aumont, O., Bopp, L., Bullister, J. L., Danabasoglu, G., Doney, S. C., Dunne, J. P., Dutay, J.-C., Graven, H., Griffies, S. M., John, J. G., Joos, F., Levin, I., Lindsay, K., Matear, R. J., McKinley, G. A., Mouchet, A., Oschlies, A., Romanou, A., Schlitzer, R., Tagliabue, A., Tanhua, T. and Yool, A.: Biogeochemical protocols and diagnostics for the CMIP6 Ocean Model Intercomparison Project (OMIP), Geosci. Model Dev., 10(6), 2169–2199, doi:10.5194/gmd-10-2169-2017, 2017.

15 Osman, M. B., Das, S. B., Trusel, L. D., Evans, M. J., Fischer, H., Grieman, M. M., Kipfstuhl, S., McConnell, J. R. and Saltzman, E. S.: Industrial-era decline in subarctic Atlantic productivity, Nature, 569(7757), 551–555, doi:10.1038/s41586-019-1181-8, 2019.

Paris, R. and Desboeufs, K. V.: Effect of atmospheric organic complexation on iron-bearing dust solubility, Atmos. Chem. Phys., 13(9), 4895–4905, doi:10.5194/acp-13-4895-2013, 2013.

20 Paris, R., Desboeufs, K. V. and Journet, E.: Variability of dust iron solubility in atmospheric waters: Investigation of the role of oxalate organic complexation, Atmos. Environ., 45(36), 6510–6517, doi:10.1016/j.atmosenv.2011.08.068, 2011.

Prospero, J. M. and Lamb, P. J.: African Droughts and Dust Transport to the Caribbean: Climate Change Implications, Science (80-.)., 302(5647), 1024–1027, doi:10.1126/science.1089915, 2003.

Le Quéré, C., Andres, R. J., Boden, T., Conway, T., Houghton, R. A., House, J. I., Marland, G., Peters, G. P., van der Werf, 25 G. R., Ahlström, A., Andrew, R. M., Bopp, L., Canadell, J. G., Ciais, P., Doney, S. C., Enright, C., Friedlingstein, P., Huntingford, C., Jain, A. K., Jourdain, C., Kato, E., Keeling, R. F., Klein Goldewijk, K., Levis, S., Levy, P., Lomas, M., Poulter, B., Raupach, M. R., Schwinger, J., Sitch, S., Stocker, B. D., Viovy, N., Zaehle, S. and Zeng, N.: The global carbon budget 1959–2011, Earth Syst. Sci. Data, 5(1), 165–185, doi:10.5194/essd-5-165-2013, 2013.

Rubin, M., Berman-Frank, I. and Shaked, Y.: Dust- and mineral-iron utilization by the marine dinitrogen-fixer Trichodesmium, 30 Nat. Geosci., 4(8), 529–534, doi:10.1038/ngeo1181, 2011.

Schneider, B., Bopp, L., Gehlen, M., Segschneider, J., Frölicher, T. L., Cadule, P., Friedlingstein, P., Doney, S. C., Behrenfeld, M. J. and Joos, F.: Climate-induced interannual variability of marine primary and export production in three global coupled climate carbon cycle models, Biogeosciences, 5(2), 597–614, doi:10.5194/bg-5-597-2008, 2008.

Schulz, M., Prospero, J. M., Baker, A. R., Dentener, F., Ickes, L., Liss, P. S., Mahowald, N. M., Nickovic, S., García-Pando,

C. P., Rodríguez, S., Sarin, M., Tegen, I. and Duce, R. A.: Atmospheric Transport and Deposition of Mineral Dust to the Ocean: Implications for Research Needs, Environ. Sci. Technol., 46(19), 10390–10404, doi:10.1021/es300073u, 2012.

Shi, Z., Krom, M. D., Bonneville, S., Baker, A. R., Bristow, C., Drake, N., Mann, G., Carslaw, K., McQuaid, J. B., Jickells, T. and Benning, L. G.: Influence of chemical weathering and aging of iron oxides on the potential iron solubility of Saharan dust during simulated atmospheric processing, Global Biogeochem. Cycles, 25(2), GB2010, doi:10.1029/2010GB003837, 2011.

Skyllas, N., Bintanja, R., Buma, A. G. J., Brussaard, C. P. D., Gröger, M., Hieronymus, J. and van de Poll, W. H.: Validation of Stratification-Driven Phytoplankton Biomass and Nutrient Concentrations in the Northeast Atlantic Ocean as Simulated by EC-Earth, Geosciences, 9(10), 450, doi:10.3390/geosciences9100450, 2019.

Smith, H. J.: The state of ocean CO_2 uptake, edited by S. Hurtley, Science (80-.)., 363(6432), 1187.2-1187, doi:10.1126/science.363.6432.1187-b, 2019.

Steinacher, M., Joos, F., Frölicher, T. L., Bopp, L., Cadule, P., Cocco, V., Doney, S. C., Gehlen, M., Lindsay, K., Moore, J. K., Schneider, B. and Segschneider, J.: Projected 21st century decrease in marine productivity: a multi-model analysis, Biogeosciences, 7(3), 979–1005, doi:10.5194/bg-7-979-2010, 2010.

Tagliabue, A., Mtshali, T., Aumont, O., Bowie, A. R., Klunder, M. B., Roychoudhury, A. N. and Swart, S.: A global compilation of dissolved iron measurements: focus on distributions and processes in the Southern Ocean, Biogeosciences, 9(6), 2333–2349, doi:10.5194/bg-9-2333-2012, 2012.

Tagliabue, A., Aumont, O. and Bopp, L.: The impact of different external sources of iron on the global carbon cycle, Geophys. Res. Lett., 41(3), 920–926, doi:10.1002/2013GL059059, 2014.

Tagliabue, A., Aumont, O., Death, R., Dunne, J. P., Dutkiewicz, S., Galbraith, E., Misumi, K., Moore, J. K., Ridgwell, A., Sherman, E., Stock, C., Vichi, M., Völker, C. and Yool, A.: How well do global ocean biogeochemistry models simulate dissolved iron distributions?, Global Biogeochem. Cycles, 30(2), 149–174, doi:10.1002/2015GB005289, 2016.

Tagliabue, A., Bowie, A. R., Boyd, P. W., Buck, K. N., Johnson, K. S. and Saito, M. A.: The integral role of iron in ocean biogeochemistry, Nature, 543(7643), 51–59, doi:10.1038/nature21058, 2017.

Tegen, I., Harrison, S. P., Kohfeld, K., Prentice, I. C., Coe, M. and Heimann, M.: Impact of vegetation and preferential source areas on global dust aerosol: Results from a model study, J. Geophys. Res. Atmos., 107(D21), AAC 14-1-AAC 14-27, doi:10.1029/2001JD000963, 2002.

Tsigaridis, K., Krol, M., Dentener, F. J., Balkanski, Y., Lathière, J., Metzger, S., Hauglustaine, D. A. and Kanakidou, M.: Change in global aerosol composition since preindustrial times, Atmos. Chem. Phys., 6(12), 5143–5162, doi:10.5194/acp-6-5143-2006, 2006.

van Vuuren, D. P., Edmonds, J., Kainuma, M., Riahi, K., Thomson, A., Hibbard, K., Hurtt, G. C., Kram, T., Krey, V., Lamarque, J.-F., Masui, T., Meinshausen, M., Nakicenovic, N., Smith, S. J., Rose, S. K., Vuuren, D. P. Van, Edmonds, J., Kainuma, M., Riahi, K., Nakicenovic, N., Smith, S. J. and Rose, S. K.: The representative concentration pathways: an overview, Clim. Change, 109(1–2), 5–31, doi:10.1007/s10584-011-0148-z, 2011.

Wang, R., Balkanski, Y., Boucher, O., Ciais, P., Peñuelas, J. and Tao, S.: Significant contribution of combustion-related emissions to the atmospheric phosphorus budget, Nat. Geosci., 8(1), 48–54, doi:10.1038/ngeo2324, 2014.

Wang, R., Balkanski, Y., Bopp, L., Aumont, O., Boucher, O., Ciais, P., Gehlen, M., Peñuelas, J., Ethé, C., Hauglustaine, D., Li, B., Liu, J., Zhou, F. and Tao, S.: Influence of anthropogenic aerosol deposition on the relationship between oceanic productivity and warming, Geophys. Res. Lett., 42(24), 10745–10754, doi:10.1002/2015GL066753, 2015a.

Wang, R., Balkanski, Y., Boucher, O., Bopp, L., Chappell, A., Ciais, P., Hauglustaine, D., Peñuelas, J. and Tao, S.: Sources, transport and deposition of iron in the global atmosphere, Atmos. Chem. Phys., 15(11), 6247–6270, doi:10.5194/acp-15-6247-2015, 2015b.

Wang, W.-L., Moore, J. K., Martiny, A. C. and Primeau, F. W.: Convergent estimates of marine nitrogen fixation, Nature, 566(7743), 205–211, doi:10.1038/s41586-019-0911-2, 2019.

Wanninkhof, R.: Relationship between wind speed and gas exchange over the ocean, J. Geophys. Res., 97(C5), 7373, doi:10.1029/92JC00188, 1992.

Weber, R. J., Guo, H., Russell, A. G. and Nenes, A.: High aerosol acidity despite declining atmospheric sulfate concentrations over the past 15 years, Nat. Geosci., 9(4), 282–285, doi:10.1038/ngeo2665, 2016.

Tables and Figures

Table 1: Nutrients (N, Fe, P) atmospheric inputs (Tg yr^{-1}) considered in PISCES, the nitrogen fixation (Tg-N yr^{-1}), and the primary production (Pg-C yr^{-1}) as calculated by the CTRL and ORGF simulations, for PAST (1851–1870 average), PRESENT (2001–2020 average) and FUTURE (2081–2100 average).

Period	Atmospheric Input Tg yr^{-1}			Nitrogen Fixation Tg-N yr^{-1}		Primary Production Pg-C yr^{-1}	
	Nutrient	CTRL	ORGF	CTRL	ORGF	CTRL	ORGF
PAST	DN	19.74	34.48	111.57	112.16	45.5	46.5
	DFe	0.18	0.23				
	DP	0.06	0.11				
PRESENT	DN	40.01	58.01	111.82	111.36	46.7	47.8
	DFe	0.28	0.35				
	DP	0.10	0.15				
FUTURE	DN	34.62	51.08	110.70	110.60	46.4	47.5
	DFe	0.24	0.30				
	DP	0.08	0.13				
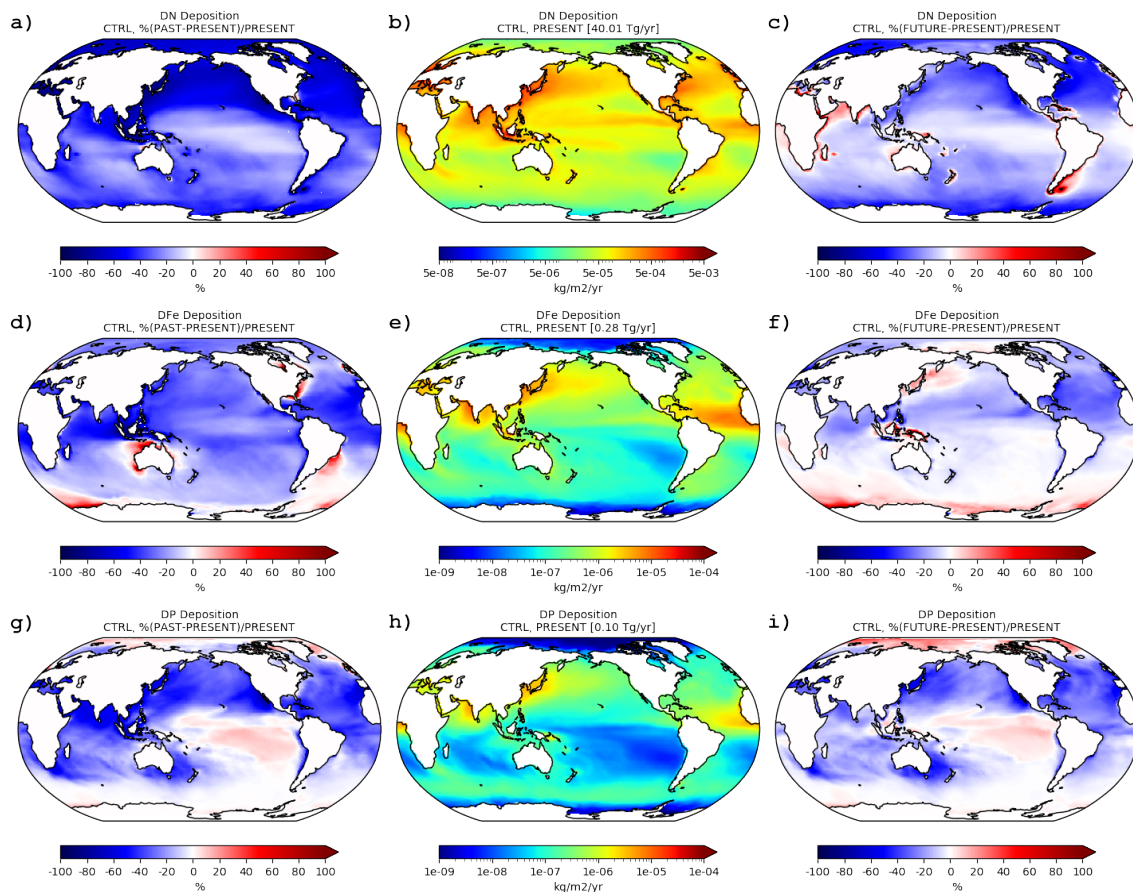
Figure 1: Atmospheric deposition fluxes into the ocean (kg m^{-2} yr^{-1}) of dissolved nitrogen (a,b,c), iron (d,e,f) and phosphorus (g,h,i) considered by the model for PRESENT (middle column), and the respective relative differences (%) to PAST (left column) and FUTURE (right column) for the CTRL simulation.
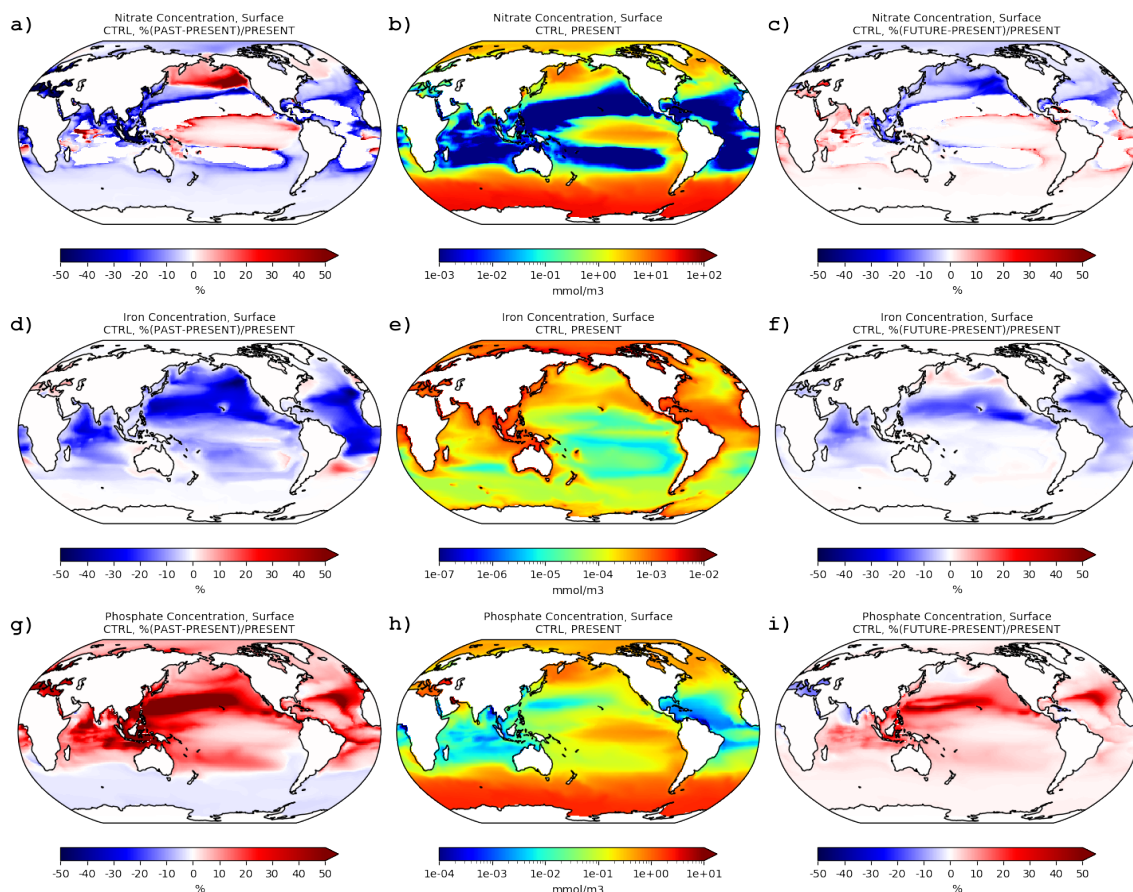
Figure 2: Surface oceanic concentrations (mmol m⁻³) of nitrate (a,b,c), iron (d,e,f) and phosphate (g,h,i) as calculated by the model for PRESENT (middle column), and the respective relative differences (%) to PAST (left column) and FUTURE (right column) for the CTRL simulation.
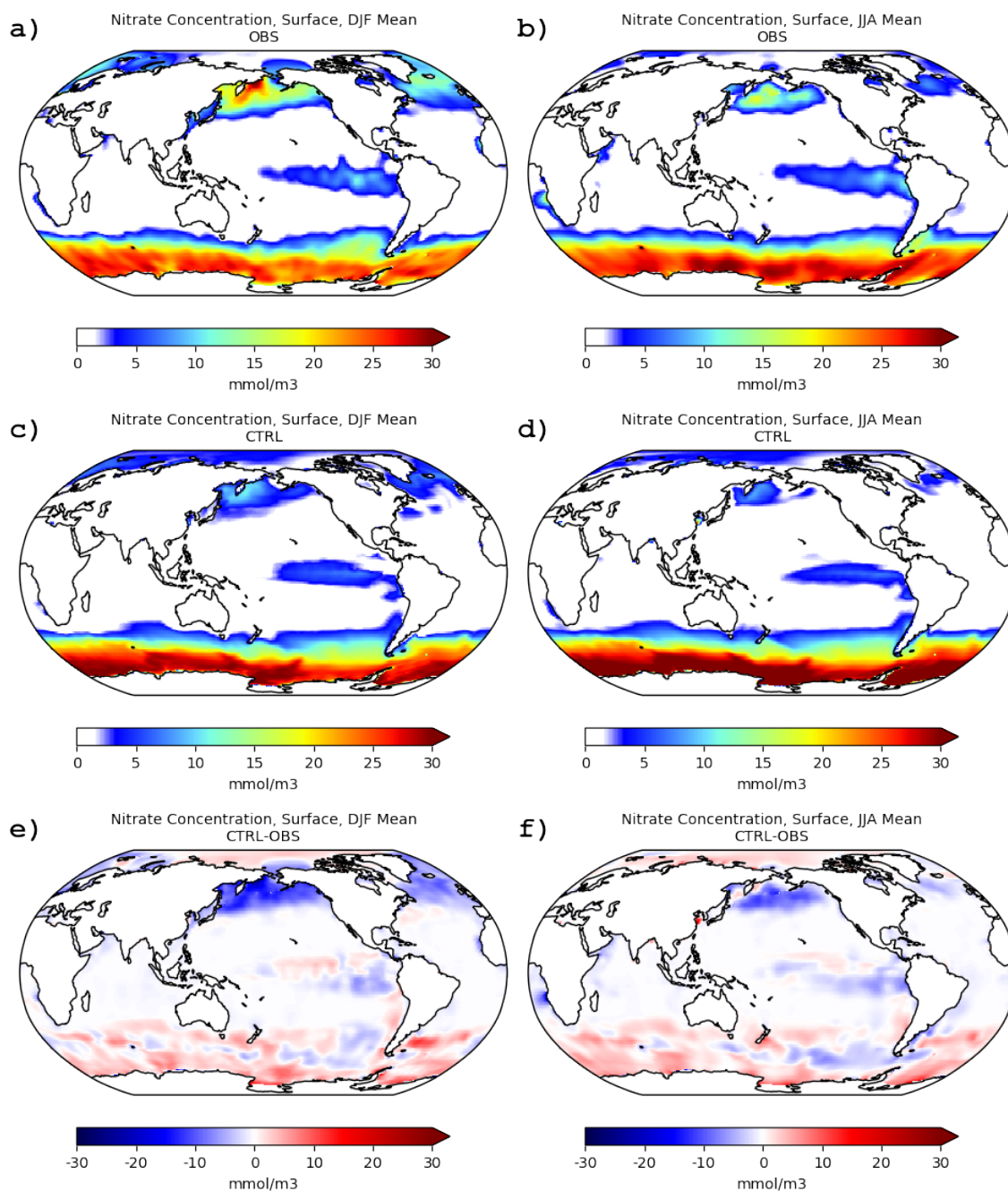
Figure 3: Surface nitrate concentrations (mmole m⁻³) for the boreal winter (DJF; left column) and summer (JJA; right column) seasons as compiled from the World Ocean Atlas (WOA; Garcia et al., 2010b) (a,b), the simulated concentrations for PRESENT as simulated for CTRL (c,d), and the absolute differences compared to observations (e,f); observational and modelled data have been averaged over a 1°x1° horizontal resolution.
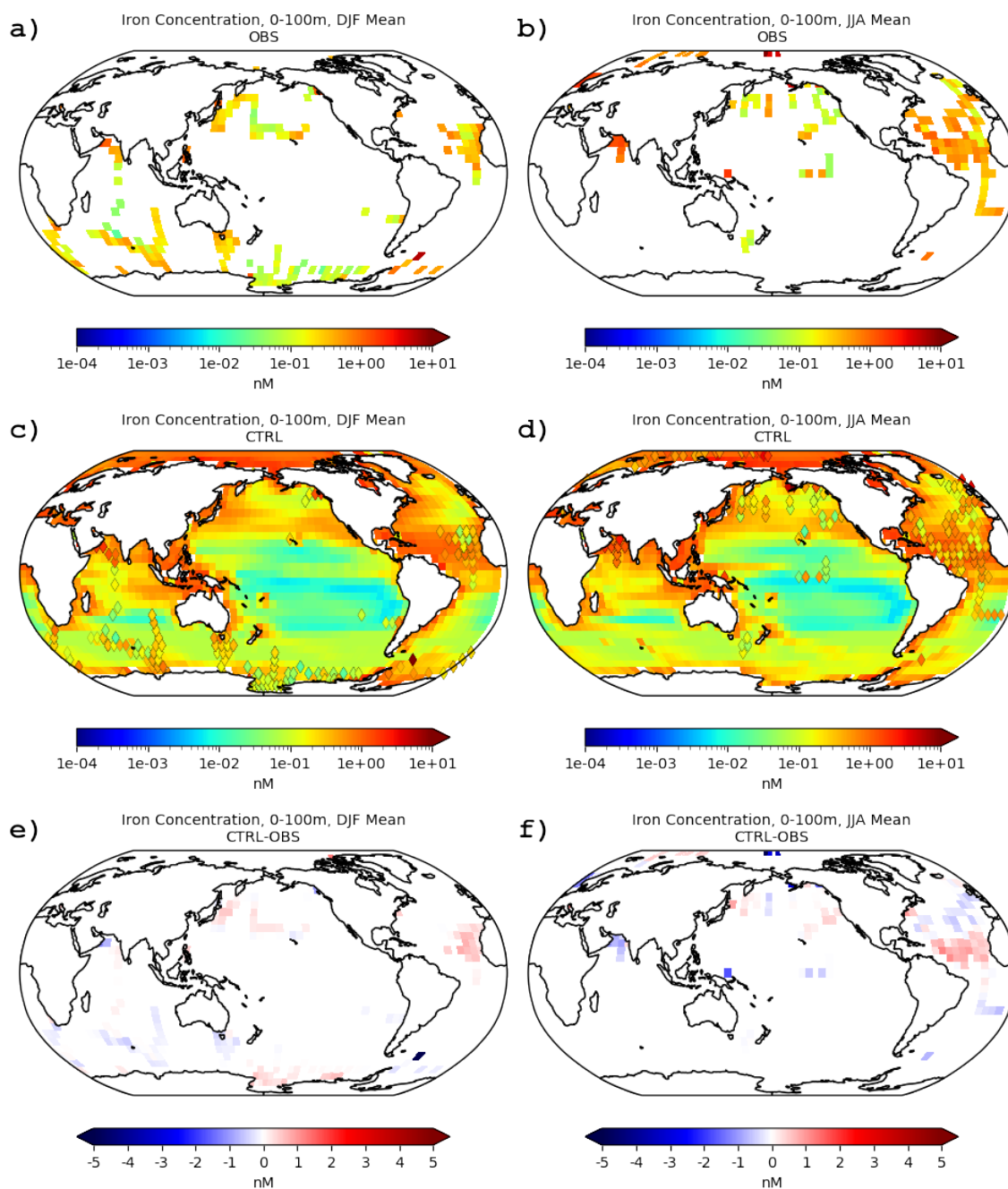
Figure 4: Iron concentrations (nM) averaged over the upper 100m for the boreal winter (DJF; left column) and summer (JJA; right column) seasons (a,b) as compiled by Tagliabue et al. (2012) (OBS), the respective simulated concentrations for PRESENT (c,d) as simulated for CTRL (diamond symbols represent observation data), and the respective absolute differences (e,f); observational and
5 **modelled data have been averaged over a 5°x5° horizontal resolution.**
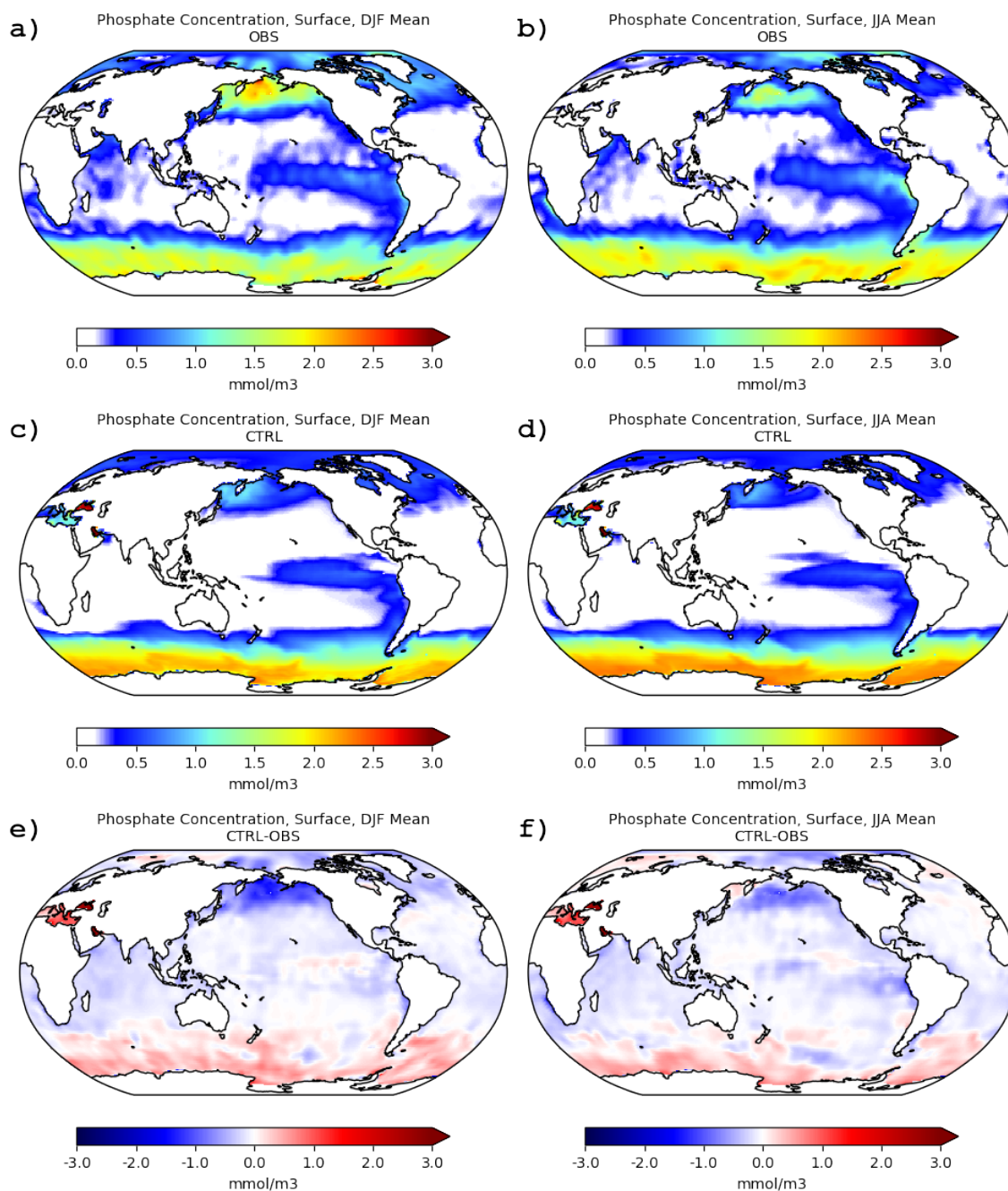
Figure 5: Surface phosphate concentrations (mmole m⁻³) for the boreal winter (DJF; left column) and summer (JJA; right column) seasons as compiled from the World Ocean Atlas (WOA; Garcia et al., 2010b) (a,b), the simulated present day surface concentrations for PRESENT as simulated for CTRL (c,d), and the respective absolute differences (e,f); observational and modelled data have been averaged over a 1°x1° horizontal resolution.
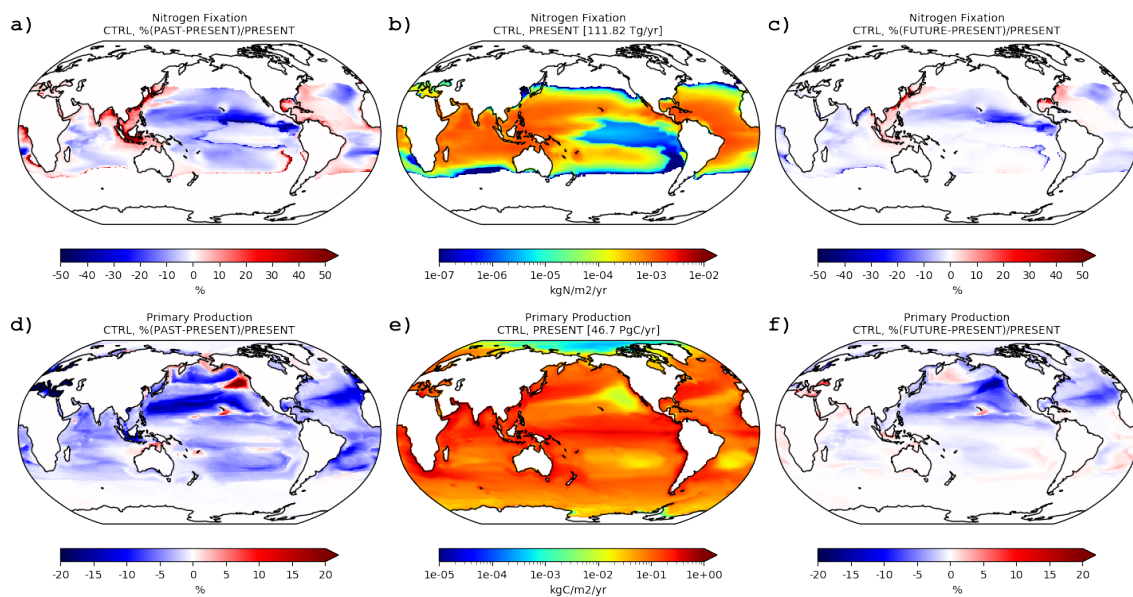
Figure 6: Nitrogen fixation (kg-N m⁻² yr⁻¹) and primary production (kg-C m⁻² yr⁻¹) rates as calculated by the model for PRESENT (b,e), and the respective relative differences (%) to PAST (a,d) and FUTURE (c,f) for the CTRL simulation.
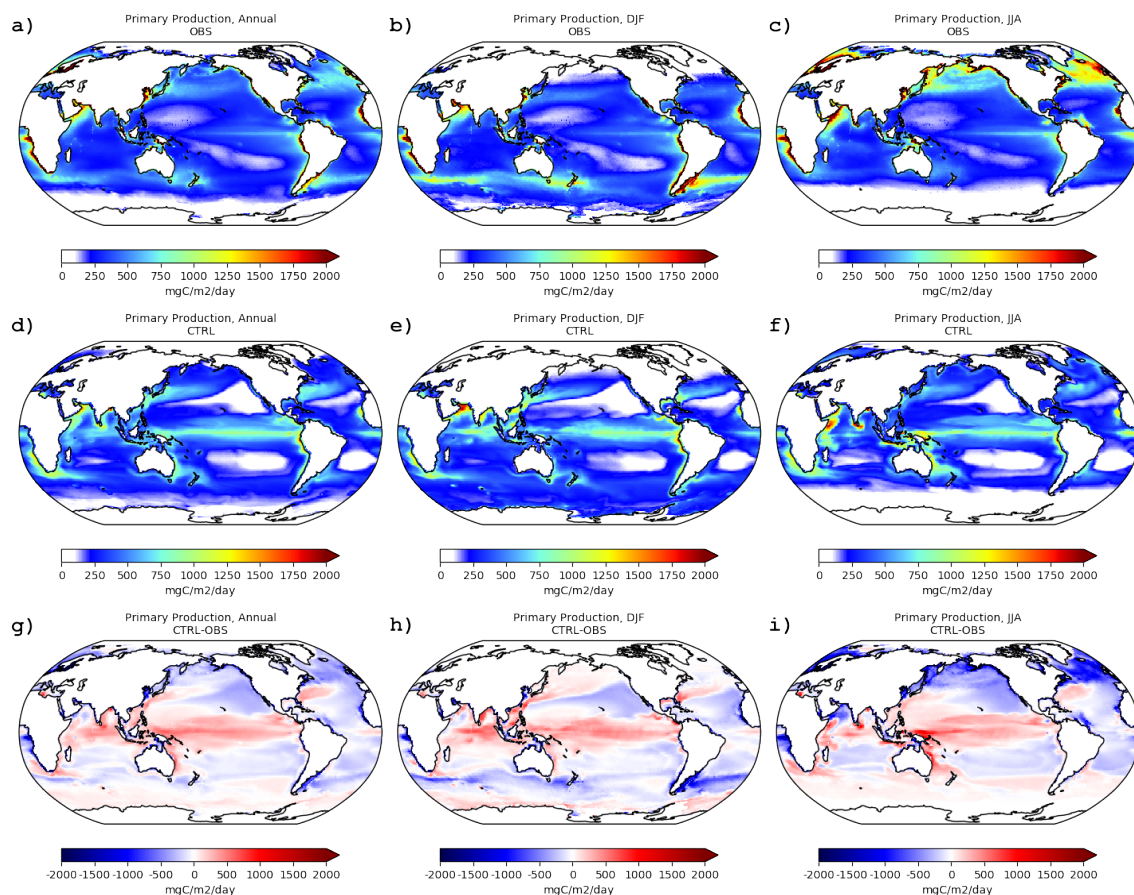
Figure 7: Primary production (mg-C m⁻² day⁻¹) for annual (left column), boreal winter (DJF; middle column) and summer (JJA; right column) seasons, as derived based on satellite-based estimates from SeaWiFS (Behrenfeld et al., 2005) (a,b,c), the simulated integrated primary production for the CTRL simulation for PRESENT (d,e,f), and the respective absolute differences (g,h,i); satellite-based and modelled data have been averaged over a 1°x1° horizontal resolution.
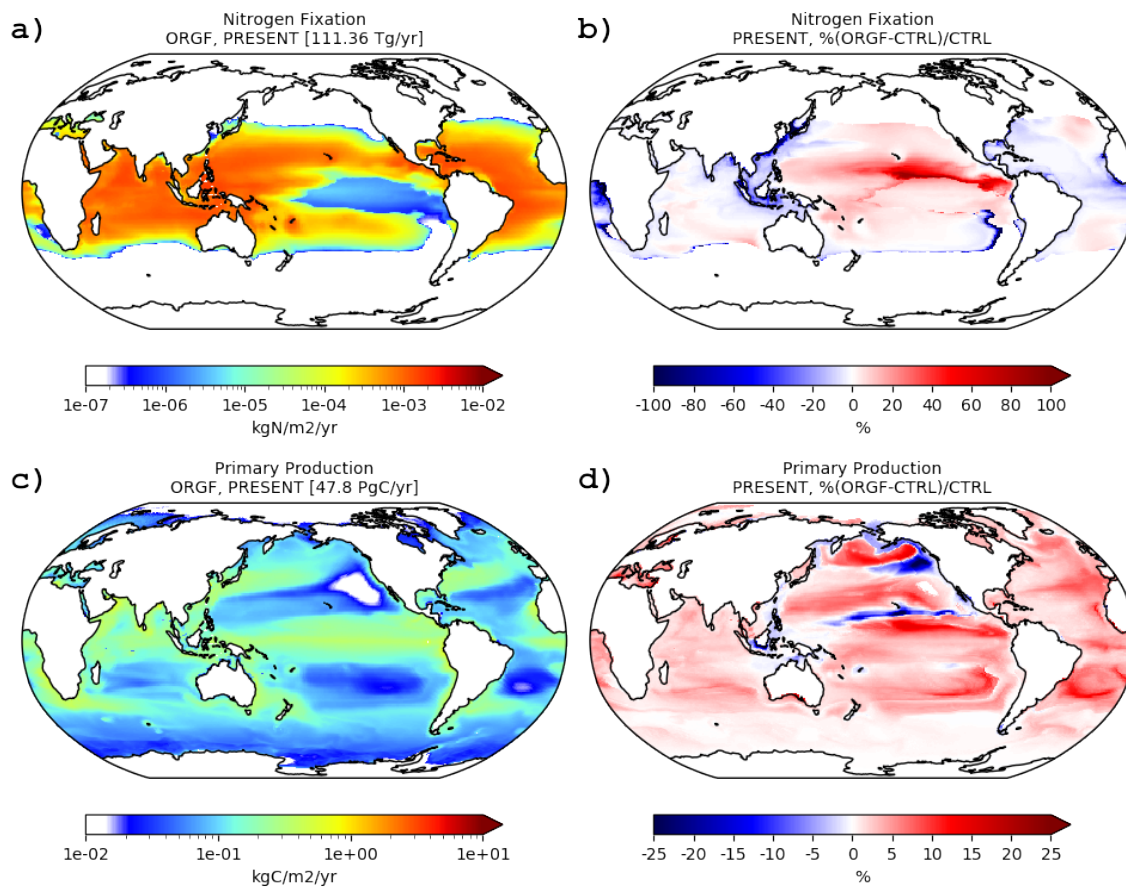
Figure 8: Nitrogen fixation (kg-N m⁻² yr⁻¹) and primary production (kg-C m⁻² yr⁻¹) rates as calculated by the model (a,c) for the ORGF simulation for PRESENT (2001–2020 average), and the respective relative (%) differences (b,d) compared to the CTRL simulation.